



## Mass distribution in the quasi-mono-energetic neutron-induced fission of $^{238}\text{U}$

H. Naik <sup>a,\*</sup>, V.K. Mulik <sup>b</sup>, P.M. Prajapati <sup>c</sup>, B.S. Shivasankar <sup>d</sup>,  
S.V. Suryanarayana <sup>e</sup>, K.C. Jagadeesan <sup>f</sup>, S.V. Thakare <sup>f</sup>, S.C. Sharma <sup>e</sup>,  
A. Goswami <sup>a</sup>

<sup>a</sup> Radiochemistry Division, Bhabha Atomic Research Centre, Mumbai 400 085, India

<sup>b</sup> Department of Physics, University of Pune, 411 007, India

<sup>c</sup> Physics Department, Faculty of Science, The M. S. University of Baroda, Vadodra 390 002, India

<sup>d</sup> Department of Statistics, Manipal University, Manipal 576 104, India

<sup>e</sup> Nuclear Physics Division, Bhabha Atomic Research Centre, Mumbai 400 085, India

<sup>f</sup> Radiopharmaceutical Division, Bhabha Atomic Research Centre, Mumbai 400 085, India

Received 19 March 2013; received in revised form 24 May 2013; accepted 24 May 2013

Available online 17 June 2013

### Abstract

The yields of various fission products in the 3.72, 5.42, 7.75 and 10.09 MeV quasi-mono-energetic neutron-induced fission of  $^{238}\text{U}$  fission have been determined using off-line  $\gamma$ -ray spectrometric technique. The mass-chain yields were obtained from their fission product yields using charge distribution correction. The peak-to-valley (P/V) ratio, the average value of light mass ( $\langle A_L \rangle$ ), heavy mass ( $\langle A_H \rangle$ ) and the average number of neutrons ( $\langle \nu \rangle$ ) at four different neutron energies of present work and at other energies from literature in the  $^{238}\text{U}(n, f)$  were obtained from the mass yield data. The present and the existing literature data in  $^{238}\text{U}(n, f)$  at various energies were compared with the similar data in the  $^{232}\text{Th}(n, f)$ . The following observations were obtained: (i) The mass yield distribution in  $^{238}\text{U}(n, f)$  is double humped unlike in the  $^{232}\text{Th}(n, f)$ , where it is triple humped. (ii) The yields of fission products for  $A = 133\text{--}134$ ,  $A = 138\text{--}139$ , and  $A = 143\text{--}144$  and their complementary products in the  $^{238}\text{U}(n, f)$  at four neutron energies are higher than those of other fission products as in the  $^{232}\text{Th}(n, f)$ . The fine structure in the mass yield distribution has been explained from the point of view of standard I and standard II asymmetric mode of fission besides even–odd effect. (iii) The yields of fission products for  $A = 133\text{--}134$  are higher in the  $^{238}\text{U}(n, f)$  than in the  $^{232}\text{Th}(n, f)$ , whereas it is reversed for  $A = 143\text{--}144$ . This has been explained from the point of shell combination of complementary fragments. (iv) In both the  $^{238}\text{U}(n, f)$  and  $^{232}\text{Th}(n, f)$ , the yields of symmetric

\* Corresponding author.

E-mail address: [naikhbarc@yahoo.com](mailto:naikhbarc@yahoo.com) (H. Naik).

products increase with excitation energy, which causes the decrease of peak-to-valley (P/V) ratio with excitation energy. (v) At the same excitation energy, the yields of symmetric products are lower in the  $^{238}\text{U}(n, f)$  than in the  $^{232}\text{Th}(n, f)$ . This causes higher value of P/V in  $^{238}\text{U}(n, f)$  than in  $^{232}\text{Th}(n, f)$  for same excitation energy. (vi) The approach of symmetric split with excitation energy is slower in the  $^{238}\text{U}(n, f)$  than in the  $^{232}\text{Th}(n, f)$ . This is due to the different type of potential energy surface for the fissioning system  $^{233}\text{Th}^*$  than in the fissioning system  $^{239}\text{U}^*$ .

© 2013 Elsevier B.V. All rights reserved.

**Keywords:** NUCLEAR REACTIONS  $^{238}\text{U}(n, f)$ ;  $E = 3.72, 5.42, 7.75, 10.09$  MeV; measured fission yields,  $E_\gamma, I_\gamma$  using off-line  $\gamma$ -spectrometry, deduced mass distributions, neutron multiplicity vs.  $E^*$ , fission yields for symmetric and asymmetric fission vs.  $E^*$ . Compared with  $^{232}\text{Th}(n, f)$  at similar energies

## 1. Introduction

Mass yield distribution studies in the low energy fission of actinides provide important information about the effect of nuclear structure besides dynamics of descent from saddle to scission point [1,2]. It is a well-known fact that the mass yield distribution [1,2] in the neutron-induced fission of pre-actinides (e.g. W, Au, Pb, Bi) and heavy-Z actinides (e.g. Es to Lr) are symmetric in nature, whereas for medium-Z actinides (e.g. U to Cf) are asymmetric in nature. On the other hand, the neutron-induced fission of light-Z actinides (e.g. Ac, Th, Pa) are asymmetric with triple humped mass yield distribution [1,2]. However, with increase of excitation energy and Z of the actinides, mass yield distribution changes from asymmetric to symmetric and the effect of nuclear structure decreases. Among the actinides, fission of Th–Pa–U and U–Np–Pu is more interesting and important for the understanding of basic fission phenomena and for their application in various types of reactors. In particular Th and U are of more interest due to their applications in accelerated driven sub-critical system (ADSs) [3–8], advanced heavy water reactor (AHWR) [9,10], conventional light and heavy water reactor and fast reactor [11–15].

Data on fission product yields relevant to mass distribution studies in the neutron-induced fission of Th and U are available in different compilations [16–20]. In the literature, some data are available in the reactor neutron-induced fission of  $^{232}\text{Th}$  [21,22] and  $^{238}\text{U}$  [23,24]. However, fission yield data for various other mono-energetic neutron-induced fissions of  $^{232}\text{Th}$  [25–48] and  $^{238}\text{U}$  [48–73] are available in literature. On the other hand, yields of fission fragments in the excitation energy range of the GDR region due to electromagnetic fission in inverse kinematics [74–76] are available for neutron-deficient lighter actinides such as  $^{220-229}\text{Th}$  and  $^{231-234}\text{U}$ .

From the above data, it can be seen that in the neutron-induced fission [16–73] of  $^{232}\text{Th}$  and  $^{238}\text{U}$ , the yields of fission products are higher around mass numbers 133–135, 138–140 and 143–145 and their complementary products depending on the mass of the fissioning systems [23,24]. However, the yields of fission products are more pronounced for  $A = 133-135$  in the  $^{238}\text{U}(n, f)$  [23,24,48–72] and for  $A = 143-145$  in the  $^{232}\text{Th}(n, f)$  [21,22,25–48]. In the electromagnetic fission of lighter actinides [74–76], the higher yields of the fission products around mass numbers 133–135 corresponding to a most probable charge of 52 have been also observed. However, from the above data it is not clear at what neutron energy the nuclear structure disappear. This is because most of the fission yields data available in systematic region based on off-line and  $\gamma$ -ray spectrometric technique is within neutron energy of 1.5–11.3 MeV in the  $^{238}\text{U}(n, f)$  [28,64–69] and  $^{232}\text{Th}(n, f)$  [28,41–43], except the data around 14 MeV [25–40,44–63]. At higher energy, the experimental results are available in the 33–60 MeV quasi-mono-energetic neutron-induced fission of  $^{232}\text{Th}$  and  $^{238}\text{U}$  using physical measurement [48], where effect of nu-

clear structure is not expected. Even otherwise, it is not possible to examine the nuclear structure effect on fission product yields based on the data from the physical measurement. This is because it needs the neutron emission correction to obtain the fission product yields from the fragment yields. This is not an easy task due to the unavailability of neutron emission curve. In view of this, in the present work we have determined the yields of various fission products in the 3.72, 5.42, 7.75 and 10.09 MeV quasi-mono-energetic neutron-induced fission of  $^{238}\text{U}$  using off-line  $\gamma$ -ray spectrometric technique. From the yields of the fission products, their mass-chain yields were obtained by using charge distribution correction [20,77]. The fission product yields data in the four neutron energies of the present work and at other neutron energies from literature [28, 34,48–73] in  $^{238}\text{U}(n, f)$  are compared with the similar data in  $^{232}\text{Th}(n, f)$  [25–46,48] to examine the role of excitation energy on the nuclear structure effect. The effect of excitation energy on peak-to-valley (P/V) ratio has also been discussed.

## 2. Experimental details

The experiment was carried out using the 14UD BARC-TIFR Pelletron facility at Mumbai, India [78,79]. The neutron beam was obtained from the  $^7\text{Li}(p, n)^7\text{Be}$  reaction by using the proton beam main line at 6 m height above the analyzing magnet of the Pelletron facility to utilize the maximum proton current from the accelerator. A collimator of 6 mm diameter was used before the Li target to avoid the energy spread of the proton beam. At this port, the terminal voltage is regulated by generating voltage mode (GVM) using terminal potential stabilizer. The lithium foil used for the neutron production was made up of natural lithium with thickness of 3.7 mg/cm<sup>2</sup>, sandwiched between two tantalum foils of different thickness. The front tantalum foil facing the proton beam is 3.9 mg/cm<sup>2</sup> thick, in which degradation of proton energy is only 50–80 keV [80]. On the other hand, the back tantalum foil is 0.025–0.1 mm thick, which is sufficient to stop the proton beam. Behind the Ta–Li–Ta stack, the samples used for irradiation were placed.

The samples consist of natural  $^{238}\text{U}$  metal foil wrapped with 0.025 mm thick super pure aluminum foil of purity 99.99%. The aluminum wrapper was used as a catcher foil to stop fission products recoiling out from the  $^{238}\text{U}$  metal foil during the irradiation. The size of  $^{238}\text{U}$  metal foil was 1.0 cm<sup>2</sup> with thickness of 634.2 mg/cm<sup>2</sup>. The sample was mounted at zero degree angle in the forward direction with respect to the beam direction at a distance of 2.1 cm from the location of the Ta–Li–Ta stack. Different sets of Ta–Li–Ta stacks and Al wrapped U samples were made for different irradiations at various neutron energies. The sample was then irradiated by neutrons generated by impinging the proton beam on the lithium metal foil through the thin tantalum foil of the Ta–Li–Ta metal stack. The irradiations time were for 6–4 h depending upon the energy of proton beam facing the thin tantalum target. The energies of proton beam of the present experiment were 5.6, 7.8, 12 and 18 MeV, respectively. The proton current during the irradiations varied from 200 to 400 nA. The corresponding maximum energies of the neutron beam impinging on the U samples were 3.72, 5.92, 10.12 and 16.12 MeV, respectively. After irradiation, the samples were cooled for 1–2 h. Then the irradiated targets were mounted on different Perspex plates and taken for  $\gamma$ -ray counting.

The  $\gamma$ -rays of fission products from the irradiated samples were counted in energy and efficiency calibrated 80 cm<sup>3</sup> HPGe detector coupled to a PC-based 4 K channel analyzer. The counting dead time was kept always 5% by placing the irradiated sample at a suitable distance from the end cap of the detector to avoid pileup effects. The  $\gamma$ -ray counting of the sample was done in live time mode and was followed as a function of time. The resolution of the detector system during counting was 1.8 keV FWHM at 1332.5 keV of  $^{60}\text{Co}$ . The energy and efficiency

calibration of the detector system was performed with  $\gamma$ -rays from standard  $^{152}\text{Eu}$ , chosen so to cover simultaneously the energy range from 121.8 to 1408.01 keV. The  $\gamma$ -ray counting of the standard sources were done at the same geometry keeping in mind the summation error. The detector efficiency was 20% at 1332.5 keV relative to 3" diameter x3" length NaI(Tl) detector. The uncertainty in the efficiency was 2–3%. For each irradiated samples several sets of measurements were done with increasing counting time to cover the different fission products, from the half-life of 30 minutes to 284 days. The  $\gamma$ -ray counting of the irradiated U samples was done up to few months to check the half-life of the fission products of interest.

### 3. Calculation and results

#### 3.1. Calculation of the neutron energy

In the present experiment, the neutron flux was produced from the  $^7\text{Li}(p, n)$  reaction. In natural lithium, the isotopic abundances of  $^6\text{Li}$  and  $^7\text{Li}$  are 7.59% and 92.41%, respectively. The Reactions of proton with natural lithium to produce neutrons [81–83] are as follows:

No.	Reaction	$Q$ -value (MeV)	Threshold energy (MeV)
1.	$^6\text{Li}(p, n)^6\text{Be}$	–5.07	5.92
2.	$^6\text{Li}(p, np)^5\text{Be}$	–5.67	6.62
3.	$^7\text{Li}(p, n)^7\text{Be}$ (ground-state transition)	–1.644	1.881
4.	$^7\text{Li}(p, n)^7\text{Be}^*$ (first excited-state transition)	–2.079	2.38
5.	$^7\text{Li}(p, n^3\text{He})^4\text{He}$ (three-body break up reaction)	–3.23	3.6
6.	$^7\text{Li}(p, n)^7\text{Be}^{**}$	–6.18	7.06

Among the above, reactions 3, 4 and 5 primarily contribute to the number of neutrons, while reactions 1, 2 and 6 do not contribute significantly. It is known that the ratio of the yield from reaction 6 to that from reaction 3 is only about 2% for  $E_p = 9$  MeV and it is presumably smaller at lower energies [83]. The low abundance of  $^6\text{Li}$  and small cross-section would lead to small contributions for reactions 1 and 2. It can be seen from the above reactions that the  $Q$ -value for the  $^7\text{Li}(p, n)^7\text{Be}$  reaction to the ground state is –1.644 MeV, whereas the first excited state is 0.431 MeV above ground state leading to an average  $Q$ -value of –1.868 MeV. However, the threshold value to populate the ground state of  $^7\text{Be}$  is 1.881 MeV. Thus, for the proton energies of 5.6, 7.8, 12.0 and 18.0 MeV the resulting peak energies of first group of neutrons ( $n_0$ ) will be 3.72, 5.92, 10.12 and 16.12 MeV, respectively. The corresponding neutron energies of second group of neutrons ( $n_1$ ), for the first excited state of  $^7\text{Be}$  will be 3.23, 5.43, 9.63 and 15.63 MeV, respectively. This is because above 2.37 MeV, the  $n_1$  group of neutron is also produced. The branching ratio to the ground state and first excited state of  $^7\text{Be}$  up to  $E_p = 7$  MeV is given by Liskien and Paulsen [81]. Similarly, Meadows and Smith [82] have also given the branching ratio to the ground state and first excited state of  $^7\text{Be}$  up to 7 MeV. On the other hand, Poppe et al. [83] have given the branching ratio to the ground state and first excited state of  $^7\text{Be}$  for  $E_p = 4.2$  MeV to 26 MeV. Above proton energy of 4.5 MeV, the fragmentation of  $^8\text{Be}$  to  $^4\text{He} + ^3\text{He} + n$  ( $Q = -3.23$  MeV) takes place and other reaction channels open up, leading to a continuous neutron energy distribution besides  $n_0$  and  $n_1$  groups of neutrons. Meadows and Smith [82] have given experimental neutron distributions from the break up channels and also parameterized these distributions. We have generated the neutron spectrum using the neutron energy distribution given by Poppe et al. [83] and shown in our earlier work [78,79]. From those

neutron spectrums [78,79], the flux-weighted average neutron energies were calculated as 3.72, 5.42, 7.75 and 10.09 MeV, respectively. The energy spread for the above average neutron energies are around 0.3 to 0.7 MeV [78,79].

### 3.2. Calculation of fission product yields

The observed photo-peak areas ( $N_{\text{obs}}$ ) of different  $\gamma$  rays of the fission products of interest were obtained by subtracting the linear Compton background from their total peak areas. From the observed number of detected  $\gamma$ -rays ( $N_{\text{obs}}$ ) under the photo-peak of an individual fission product, their cumulative yields ( $Y_{\text{R}}$ ) relative to  $^{135}\text{I}$  were calculated by using the standard decay equation [23,24],

$$Y_{\text{R}} = \frac{N_{\text{obs}}(T_{\text{CL}}/T_{\text{LT}})\lambda}{n\sigma_f\phi I_{\gamma}\varepsilon(1 - e^{-\lambda t_{\text{irr}}})e^{-\lambda t_{\text{cool}}}(1 - e^{-\lambda T_{\text{CL}}})} \quad (1)$$

where  $n$  is the number of target atoms,  $\phi$  is the neutron flux and  $\sigma_f$  is the neutron-induced fission cross section of  $^{238}\text{U}$  at 3.72, 5.42, 7.75 and 10.09 MeV.  $I_{\gamma}$  is the branching ratio or intensity of the  $\gamma$  ray,  $\varepsilon$  is the detection efficiency of the  $\gamma$  rays in the detector system and  $\lambda$  is the decay constant of the fission product of interest ( $\lambda = \ln 2/T_{1/2}$ ).  $t_{\text{irr}}$  and  $t_{\text{cool}}$  are the irradiation and cooling times, whereas,  $T_{\text{CL}}$  and  $T_{\text{LT}}$  are the real time and the live time of counting, respectively. The nuclear spectroscopic data, such as the  $\gamma$ -ray energies, the half-lives ( $T_{1/2}$ ), and the  $\gamma$ -ray intensity ( $I_{\gamma}$ ) of the fission products were taken from the literature [84,85].

From the relative cumulative yields ( $Y_{\text{R}}$ ) of the fission products, their relative mass-chain yields ( $Y_{\text{A}}$ ) were calculated by using Wahl's prescription of charge distribution [20]. According to this, the fractional cumulative yield ( $Y_{\text{FCY}}$ ) of a fission product in an isobaric mass-chain is given as

$$Y_{\text{FCY}} = \frac{\text{EOF}^{a(Z)}}{\sqrt{2\pi\sigma^2}} \int_{-\infty}^{Z+0.5} \exp[-(Z - Z_{\text{P}})^2/2\sigma^2] dZ \quad (2)$$

$$Y_{\text{A}} = Y_{\text{R}}/Y_{\text{FCY}} \quad (3)$$

where  $Z_{\text{P}}$  is the most probable charge and  $\sigma_z$  is the width parameter of an isobaric-yield distribution.  $\text{EOF}^{a(Z)}$  is the even-odd effect with  $a(Z) = +1$  for even- $Z$  nuclides and  $-1$  for odd- $Z$  nuclides.

It can be seen from the above equation that in an isobaric mass-chain, it is necessary to have knowledge of  $Z_{\text{P}}$ ,  $\sigma_z$  and  $\text{EOF}^{a(Z)}$  to calculate the  $Y_{\text{FCY}}$  value of a fission product and a mass-chain yield. The  $\text{EOF}^{a(Z)}$  values in the medium energy fission is negligible. The  $\sigma_z$  value of  $0.70 \pm 0.06$  in medium energy proton and alpha-induced fission of  $^{232}\text{Th}$  and  $^{238}\text{U}$  was obtained by Umezawa et al. [77]. The  $Z_{\text{P}}$  values of individual mass-chain ( $A$ ) for the above fission systems were calculated using the prescription of Umezawa et al. [77], which is given below:

$$Z_{\text{P}} = \eta Z_{\text{F}} \pm \Delta Z_{\text{P}}, \quad \eta Z_{\text{F}} = Z_{\text{UCD}} = (Z_{\text{F}}/A_{\text{F}})(A + \nu_{\text{post}}) \quad (4a)$$

$$\eta = (A + \nu_{\text{post}})/(A_{\text{C}} - \nu_{\text{pre}}), \quad A_{\text{F}} = A_{\text{C}} - \nu_{\text{pre}} \quad (4b)$$

where  $Z_{\text{C}}$  and  $A_{\text{C}}$  are the charge and mass of the compound nucleus.  $Z_{\text{F}}$  and  $A_{\text{F}}$  are the charge and mass of the fissioning system.  $Z_{\text{UCD}}$  is the most probable charge based on the unchanged charge-density distribution as suggested by Sugarman and Turkevich [86].  $A$  is the mass of the

fission product, whereas  $\nu_{\text{pre}}$  and  $\nu_{\text{post}}$  are pre- and post-fission neutrons.  $\Delta Z_{\text{P}}$  ( $= Z_{\text{P}} - Z_{\text{UCD}}$ ) is the charge-polarization parameter. The + and – signs for the  $\Delta Z_{\text{P}}$  value are applicable to light and heavy fragments, respectively.

The pre- ( $\nu_{\text{pre}}$ ) and post- ( $\nu_{\text{post}}$ ) scission neutrons can be calculated as [77]

$$\nu_{\text{pre}} = \frac{E^*}{7.5 \pm 0.5} + \frac{Z_{\text{C}}}{2A_{\text{C}}} - (19.0 \pm 0.5)$$

1.0 for  $A > 88$  (5a)

$$\nu_{\text{post}} = 1.0 + 0.1(A - 88) \quad \text{for } 78 < A < 88$$

0 for  $A < 78$  (5b)

where  $E^*$  is the excitation energy of the compound nucleus. For the neutron energies of 3.72, 5.42, 7.75 and 10.09 MeV, the excitation energies of the compound nucleus are 8.53, 10.23, 12.56 and 14.9 MeV, respectively. The excitation energies were used in Eq. (5a) to calculate the  $\nu_{\text{pre}}$  values at three different neutron energies. The values of  $\nu_{\text{pre}}$  and  $\nu_{\text{post}}$  obtained based on Eqs. (5a) and (5b) were used in Eqs. (4a) and (4b) to calculate the value of  $Z_{\text{UCD}}$  as a function of mass number for the different fission products. The  $\Delta Z_{\text{P}}$  value was then calculated by using the following relation [77]:

$$\Delta Z_{\text{P}} = 0 \quad \text{for } I\eta - 0.5I < 0.04 \quad (6a)$$

$$\Delta Z_{\text{P}} = (20/3)(I\eta - 0.5I - 0.04) \quad \text{for } 0.04 < I\eta - 0.5I < 0.085 \quad (6b)$$

The  $Z_{\text{P}}$  value as a function of mass number and the average width parameter ( $\sigma_z$ ) of 0.7 were used in Eq. (2) to obtain the  $Y_{\text{FCY}}$  values for individual fission products. The  $Y_{\text{FCY}}$  values for most of the fission products in the present work are above 0.9, except for the fission products  $^{128}\text{Sn}$ ,  $^{131}\text{Sb}$ , and  $^{134}\text{Te}$ , where slight lower values were observed. The mass-chain yield ( $Y_{\text{A}}$ ) of the fission products from their relative cumulative yield ( $Y_{\text{R}}$ ) was obtained from Eq. (3) by using the  $Y_{\text{FCY}}$  values of different fission products. The relative mass-chain yields of the fission products obtained were then normalized to a total yield of 200% to calculate the absolute mass-chain yields. The absolute cumulative yields of the fission products in the 3.72-, 5.42-, 7.75- and 10.09-MeV neutron-induced fission of  $^{232}\text{Th}$  were then obtained by using the mass yield data and  $Y_{\text{FCY}}$  values. The relative cumulative yield ( $Y_{\text{R}}$ ) and mass-chain yield ( $Y_{\text{A}}$ ) of the fission products in the 3.72-, 5.42-, 7.75- and 10.09-MeV neutron-induced fission of  $^{238}\text{U}$  along with the nuclear spectroscopic data from Refs. [84,85] are given in Tables 1, 2, 3 and 4, respectively. The absolute mass-chain yields in the neutron-induced fission of  $^{238}\text{U}$  from the present work for the above mentioned four neutron energies are also given in the last columns of Tables 1–4. The uncertainty shown in the measured cumulative yield of the individual fission products shown in Tables 1–4 is the statistical fluctuation of the mean value from two determinations. The overall uncertainty represents contributions from both random and systematic errors. The random error in the observed activity is due to counting statistics and is estimated to be 5%–10%, which can be determined by accumulating the data for the optimum period of time, depending on the half-life of the nuclide of interest. On the other hand, the systematic errors are due to the uncertainties in irradiation time (0.2%), detector efficiency calibration ( $\sim 3\%$ ), half-life of the fission products ( $\sim 1\%$ ), and  $\gamma$ -ray abundance ( $\sim 2\%$ ), which are the largest variation in the literature [84,85]. Thus, the overall systematic error is about 3.8%. An upper limit of error of 6.3%–10.7% was determined at for the fission-product yields based on 5%–10% random error and a 3.8% systematic error.

Table 1

Nuclear spectroscopic data and yields of fission products in the 3.72 MeV neutron-induced fission of  $^{238}\text{U}$ .

Nuclide	Half-life	$\gamma$ -ray		$Y_{\text{R}}$ (%)	$Y_{\text{A}}$ (%)
		Energy (keV)	Abundance (%)		
$^{84}\text{Br}$	31.8 min	1616.2	6.2	$0.743 \pm 0.098$	$0.743 \pm 0.098$
$^{85}\text{Kr}^{\text{m}}$	4.48 h	151.2	75.0	$0.913 \pm 0.033$	$0.913 \pm 0.033$
		304.9	14.0	$0.891 \pm 0.025$	$0.891 \pm 0.025$
$^{87}\text{Kr}$	76.3 min	402.6	49.6	$1.494 \pm 0.121$	$1.494 \pm 0.121$
$^{88}\text{Kr}$	2.84 h	196.3	25.9	$1.951 \pm 0.064$	$1.951 \pm 0.065$
$^{91}\text{Sr}$	9.63 h	749.8	23.6	$3.440 \pm 0.206$	$3.440 \pm 0.206$
		1024.3	33.0	$3.755 \pm 0.284$	$3.755 \pm 0.284$
$^{92}\text{Sr}$	2.71 h	1384.9	90.0	$3.603 \pm 0.261$	$3.608 \pm 0.262$
$^{93}\text{Y}$	10.18 h	266.9	7.3	$3.125 \pm 0.291$	$3.125 \pm 0.291$
$^{95}\text{Zr}$	64.02 d	756.7	54.0	$5.016 \pm 0.275$	$5.016 \pm 0.275$
		724.3	44.2	$5.201 \pm 0.248$	$5.201 \pm 0.248$
$^{97}\text{Zr}$	16.91 h	743.4	93.0	$6.086 \pm 0.255$	$6.097 \pm 0.256$
$^{99}\text{Mo}$	65.94 h	140.5	89.4	$5.418 \pm 0.266$	$5.418 \pm 0.266$
		739.5	12.13	$5.380 \pm 0.168$	$5.380 \pm 0.168$
$^{103}\text{Ru}$	39.26 d	497.1	90.0	$6.483 \pm 0.397$	$6.483 \pm 0.397$
$^{105}\text{Ru}$	4.44 h	724.4	47.0	$3.211 \pm 0.157$	$3.217 \pm 0.158$
$^{105}\text{Rh}$	35.36 h	319.1	19.2	$3.298 \pm 0.196$	$3.298 \pm 0.196$
$^{112}\text{Ag}$	3.13 h	617.5	43.0	$0.076 \pm 0.011$	$0.076 \pm 0.011$
$^{113}\text{Ag}$	5.37 h	298.6	10.0	$0.052 \pm 0.011$	$0.052 \pm 0.011$
$^{115}\text{Cd}^{\text{g}}$	53.46 h	336.2	45.9	$0.0326 \pm 0.0054$	$0.0326 \pm 0.0054$
$^{115}\text{Cd}^{\text{total}}$				$0.038 \pm 0.006^*$	$0.038 \pm 0.006^*$
$^{117}\text{Cd}^{\text{m}}$	3.36 h	1066.0	23.1	$0.0120 \pm 0.0022$	
		1097.3	26.0	$0.0117 \pm 0.0027$	
$^{117}\text{Cd}^{\text{g}}$	2.49 h	273.4	28.0	$0.0185 \pm 0.0033$	
$^{117}\text{Cd}^{\text{total}}$				$0.0304 \pm 0.0038$	$0.0304 \pm 0.0038$
$^{127}\text{Sb}$	3.85 d	687.0	37.0	$0.288 \pm 0.049$	$0.288 \pm 0.049$
$^{128}\text{Sn}$	59.07 min	482.3	59.0	$0.417 \pm 0.089$	$0.460 \pm 0.098$
$^{129}\text{Sb}$	4.32 h	812.4	43.0	$0.791 \pm 0.048$	$0.794 \pm 0.048$
$^{131}\text{I}$	8.02 d	364.5	81.7	$3.673 \pm 0.284$	$3.673 \pm 0.284$
$^{132}\text{Te}$	3.2 d	228.1	88.0	$4.749 \pm 0.202$	$4.776 \pm 0.203$
$^{133}\text{I}$	20.8 h	529.9	87.0	$6.977 \pm 0.287$	$6.977 \pm 0.287$
$^{134}\text{Te}$	41.8 min	566.0	18.0	$7.885 \pm 0.239$	$8.515 \pm 0.258$
		767.2	29.5	$8.004 \pm 0.267$	$8.644 \pm 0.288$
$^{135}\text{I}$	6.57 h	1131.5	22.7	$5.547 \pm 0.259$	$5.586 \pm 0.261$
		1260.4	28.9	$5.434 \pm 0.054$	$5.472 \pm 0.054$
$^{138}\text{Cs}^{\text{g}}$	33.41 min	1435.8	76.3	$7.015 \pm 0.304$	$7.015 \pm 0.304$
		1009.8	29.8	$6.102 \pm 0.242$	$6.102 \pm 0.242$
		462.8	30.7	$6.646 \pm 0.233$	$6.646 \pm 0.233$
$^{139}\text{Ba}$	83.03 min	165.8	23.7	$6.537 \pm 0.209$	$6.537 \pm 0.209$
$^{140}\text{Ba}$	12.75 d	537.3	24.4	$5.684 \pm 0.291$	$5.684 \pm 0.291$
$^{141}\text{Ce}$	32.5 d	145.4	48.0	$5.304 \pm 0.266$	$5.304 \pm 0.266$
$^{142}\text{La}$	91.1 min	641.3	47.0	$4.233 \pm 0.196$	$4.260 \pm 0.197$
$^{143}\text{Ce}$	33.03 h	293.3	42.8	$4.592 \pm 0.297$	$4.592 \pm 0.297$
$^{144}\text{Ce}$	284.89 d	133.5	11.09	$4.847 \pm 0.255$	$4.847 \pm 0.255$
$^{147}\text{Nd}$	10.98 d	531.0	13.1	$3.211 \pm 0.191$	$3.211 \pm 0.191$
$^{149}\text{Nd}$	1.728 h	211.3	25.9	$1.975 \pm 0.157$	$1.983 \pm 0.158$
		270.2	10.6	$1.902 \pm 0.212$	$1.911 \pm 0.213$
$^{151}\text{Pm}$	53.08 h	340.8	23.0	$0.999 \pm 0.049$	$0.999 \pm 0.049$
$^{153}\text{Sm}$	46.28 h	103.2	30.0	$0.434 \pm 0.082$	$0.434 \pm 0.082$

\* The yields of  $^{115}\text{Cd}^{\text{total}}$  are based on the ratio of  $^{115}\text{Cd}^{\text{g}}/^{115}\text{Cd}^{\text{m}} = 6$  from Ref. [65].  $Y_{\text{R}}$  – cumulative yields,  $Y_{\text{A}}$  – mass yields,  $^{135}\text{I}$  – fission rate monitor.

Table 2

Nuclear spectroscopic data and yields of fission products in the 5.42 MeV neutron-induced fission of  $^{238}\text{U}$ .

Nuclide	Half-life	$\gamma$ -ray		$Y_R$ (%)	$Y_A$ (%)
		Energy (keV)	Abundance (%)		
$^{84}\text{Br}$	31.8 min	1616.2	6.2	$0.755 \pm 0.038$	$0.755 \pm 0.038$
$^{85}\text{Kr}^m$	4.48 h	151.2	75.0	$0.960 \pm 0.031$	$0.960 \pm 0.031$
		304.9	14.0	$0.976 \pm 0.037$	$0.976 \pm 0.037$
$^{87}\text{Kr}$	76.3 min	402.6	49.6	$1.611 \pm 0.146$	$1.619 \pm 0.147$
$^{88}\text{Kr}$	2.84 h	196.3	25.9	$2.152 \pm 0.269$	$2.178 \pm 0.273$
$^{91}\text{Sr}$	9.63 h	749.8	23.6	$3.781 \pm 0.157$	$3.781 \pm 0.157$
		1024.3	33.0	$3.967 \pm 0.268$	$3.967 \pm 0.268$
$^{92}\text{Sr}$	2.71 h	1384.9	90.0	$3.922 \pm 0.241$	$3.926 \pm 0.241$
$^{93}\text{Y}$	10.18 h	266.9	7.3	$3.490 \pm 0.094$	$3.490 \pm 0.094$
$^{95}\text{Zr}$	64.02 d	756.7	54.0	$5.615 \pm 0.273$	$5.615 \pm 0.273$
		724.3	44.2	$5.998 \pm 0.331$	$5.998 \pm 0.331$
$^{97}\text{Zr}$	16.91 h	743.4	93.0	$6.228 \pm 0.261$	$6.235 \pm 0.262$
$^{99}\text{Mo}$	65.94 h	140.5	89.4	$5.235 \pm 0.178$	$5.235 \pm 0.178$
		739.5	12.13	$5.613 \pm 0.262$	$5.613 \pm 0.262$
$^{103}\text{Ru}$	39.26 d	497.1	90.0	$6.251 \pm 0.251$	$6.251 \pm 0.251$
$^{105}\text{Ru}$	4.44 h	724.4	47.0	$3.893 \pm 0.282$	$3.913 \pm 0.283$
$^{105}\text{Rh}$	35.36 h	319.1	19.2	$3.965 \pm 0.231$	$3.956 \pm 0.231$
$^{112}\text{Ag}$	3.13 h	617.5	43.0	$0.117 \pm 0.014$	$0.117 \pm 0.014$
$^{113}\text{Ag}$	5.37 h	298.6	10.0	$0.094 \pm 0.017$	$0.094 \pm 0.017$
$^{115}\text{Cd}^g$	53.46 h	336.2	45.9	$0.063 \pm 0.016$	$0.063 \pm 0.016$
$^{115}\text{Cd}^{\text{total}}$				$0.074 \pm 0.018^*$	$0.074 \pm 0.018^*$
$^{117}\text{Cd}^m$	3.36 h	1066.0	23.1	$0.016 \pm 0.005$	
		1097.3	26.0	$0.018 \pm 0.006$	
$^{117}\text{Cd}^g$	2.49 h	273.4	28.0	$0.042 \pm 0.011$	
$^{117}\text{Cd}^{\text{total}}$				$0.059 \pm 0.013$	$0.059 \pm 0.013$
$^{127}\text{Sb}$	3.85 d	687.0	37.0	$0.362 \pm 0.073$	$0.362 \pm 0.073$
$^{128}\text{Sn}$	59.07 min	482.3	59.0	$0.451 \pm 0.067$	$0.497 \pm 0.073$
$^{129}\text{Sb}$	4.32 h	812.4	43.0	$0.940 \pm 0.042$	$0.942 \pm 0.042$
$^{131}\text{I}$	8.02 d	364.5	81.7	$3.141 \pm 0.136$	$3.154 \pm 0.136$
$^{132}\text{Te}$	3.2 d	228.1	88.0	$4.778 \pm 0.115$	$4.802 \pm 0.115$
$^{133}\text{I}$	20.8 h	529.9	87.0	$6.841 \pm 0.211$	$6.841 \pm 0.211$
$^{134}\text{Te}$	41.8 min	566.0	18.0	$7.135 \pm 0.277$	$7.697 \pm 0.299$
		767.2	29.5	$7.311 \pm 0.171$	$7.887 \pm 0.184$
$^{135}\text{I}$	6.57 h	1131.5	22.7	$5.051 \pm 0.224$	$5.085 \pm 0.226$
		1260.4	20.3	$5.248 \pm 0.052$	$5.285 \pm 0.052$
$^{138}\text{Cs}^g$	33.41 min	1435.8	76.3	$6.804 \pm 0.226$	$6.804 \pm 0.226$
		1009.8	29.8	$6.617 \pm 0.204$	$6.617 \pm 0.204$
		462.8	30.7	$6.436 \pm 0.246$	$6.436 \pm 0.246$
$^{139}\text{Ba}$	83.03 min	165.8	23.7	$6.604 \pm 0.273$	$6.604 \pm 0.273$
$^{140}\text{Ba}$	12.75 d	537.3	35.4	$5.930 \pm 0.214$	$5.930 \pm 0.214$
$^{141}\text{Ce}$	32.5 d	145.4	20.5	$5.355 \pm 0.226$	$5.355 \pm 0.226$
$^{142}\text{La}$	91.1 min	641.3	47.0	$4.288 \pm 0.089$	$4.288 \pm 0.089$
$^{143}\text{Ce}$	33.03 h	293.3	42.8	$4.912 \pm 0.121$	$4.912 \pm 0.121$
$^{144}\text{Ce}$	284.89 d	133.5	11.09	$5.211 \pm 0.178$	$5.211 \pm 0.178$
$^{147}\text{Nd}$	10.98 d	531.0	13.1	$3.401 \pm 0.199$	$3.401 \pm 0.199$
$^{149}\text{Nd}$	1.728 h	211.3	25.9	$2.104 \pm 0.210$	$2.112 \pm 0.211$
		270.2	10.6	$2.159 \pm 0.139$	$2.167 \pm 0.140$
$^{151}\text{Pm}$	53.08 h	340.8	23.0	$0.855 \pm 0.042$	$0.855 \pm 0.042$
$^{153}\text{Sm}$	46.28 h	103.2	30.0	$0.451 \pm 0.037$	$0.451 \pm 0.037$

\* The yields of  $^{115}\text{Cd}^{\text{total}}$  are based on the ratio of  $^{115}\text{Cd}^g/^{115}\text{Cd}^m = 6$  from Ref. [65].  $Y_R$  – cumulative yields,  $Y_A$  – mass yields,  $^{135}\text{I}$  – fission rate monitor.

Table 3

Nuclear spectroscopic data and yields of fission products in the 7.75 MeV neutron-induced fission of  $^{238}\text{U}$ .

Nuclide	Half-life	$\gamma$ -ray		$Y_{\text{R}}$ (%)	$Y_{\text{A}}$ (%)
		Energy (keV)	Abundance (%)		
$^{84}\text{Br}$	31.8 min	1616.2	6.2	$0.726 \pm 0.043$	$0.726 \pm 0.043$
$^{85}\text{Kr}^{\text{m}}$	4.48 h	151.2	75.0	$0.920 \pm 0.075$	$0.920 \pm 0.075$
		304.9	14.0	$0.956 \pm 0.086$	$0.956 \pm 0.086$
$^{87}\text{Kr}$	76.3 min	402.6	49.6	$1.894 \pm 0.156$	$1.894 \pm 0.156$
$^{88}\text{Kr}$	2.84 h	196.3	25.9	$2.315 \pm 0.127$	$2.351 \pm 0.129$
$^{91}\text{Sr}$	9.63 h	749.8	23.6	$3.950 \pm 0.228$	$3.950 \pm 0.228$
		1024.3	33.0	$4.020 \pm 0.171$	$4.020 \pm 0.171$
$^{92}\text{Sr}$	2.71 h	1384.9	90.0	$4.381 \pm 0.097$	$4.385 \pm 0.097$
$^{93}\text{Y}$	10.18 h	266.9	7.3	$3.954 \pm 0.266$	$3.954 \pm 0.266$
$^{95}\text{Zr}$	64.02 d	756.7	54.0	$5.365 \pm 0.188$	$5.365 \pm 0.188$
		724.3	44.2	$5.096 \pm 0.241$	$5.096 \pm 0.241$
$^{97}\text{Zr}$	16.91 h	743.4	93.0	$5.962 \pm 0.225$	$5.968 \pm 0.225$
$^{99}\text{Mo}$	65.94 h	140.5	89.4	$5.455 \pm 0.221$	$5.455 \pm 0.221$
		739.5	12.13	$5.751 \pm 0.247$	$5.751 \pm 0.247$
$^{103}\text{Ru}$	39.26 d	497.1	90.0	$6.151 \pm 0.291$	$6.151 \pm 0.291$
$^{105}\text{Ru}$	4.44 h	724.4	47.0	$3.821 \pm 0.059$	$3.844 \pm 0.059$
$^{105}\text{Rh}$	35.36 h	319.1	19.2	$3.912 \pm 0.152$	$3.912 \pm 0.152$
$^{112}\text{Ag}$	3.13 h	617.5	43.0	$0.289 \pm 0.048$	$0.289 \pm 0.048$
$^{113}\text{Ag}$	5.37 h	298.6	10.0	$0.230 \pm 0.043$	$0.230 \pm 0.043$
$^{115}\text{Cd}^{\text{g}}$	53.46 h	336.2	45.9	$0.173 \pm 0.032$	$0.173 \pm 0.032$
$^{115}\text{Cd}^{\text{total}}$				$0.202 \pm 0.037^*$	$0.202 \pm 0.037^*$
$^{117}\text{Cd}^{\text{m}}$	3.36 h	1066.0	23.1	$0.0468 \pm 0.0086$	
		1097.3	26.0	$0.0425 \pm 0.0043$	
$^{117}\text{Cd}^{\text{g}}$	2.49 h	273.4	28.0	$0.121 \pm 0.018$	
$^{117}\text{Cd}^{\text{total}}$				$0.166 \pm 0.021$	$0.166 \pm 0.021$
$^{127}\text{Sb}$	3.85 d	687.0	37.0	$0.543 \pm 0.027$	$0.543 \pm 0.027$
$^{128}\text{Sn}$	59.07 min	482.3	59.0	$0.769 \pm 0.041$	$0.807 \pm 0.043$
$^{129}\text{Sb}$	4.32 h	812.4	43.0	$1.238 \pm 0.134$	$1.243 \pm 0.135$
$^{131}\text{I}$	8.02 d	364.5	81.7	$3.514 \pm 0.102$	$3.514 \pm 0.102$
$^{132}\text{Te}$	3.2 d	228.1	88.0	$5.558 \pm 0.234$	$5.585 \pm 0.236$
$^{133}\text{I}$	20.8 h	529.9	87.0	$6.818 \pm 0.243$	$6.818 \pm 0.243$
$^{134}\text{Te}$	41.8 min	566.0	18.0	$7.338 \pm 0.255$	$7.890 \pm 0.275$
		767.2	29.5	$7.133 \pm 0.178$	$7.670 \pm 0.179$
$^{135}\text{I}$	6.57 h	1131.5	22.7	$5.012 \pm 0.134$	$5.047 \pm 0.135$
		1260.4	28.9	$5.381 \pm 0.053$	$5.419 \pm 0.054$
$^{138}\text{Cs}^{\text{g}}$	33.41 min	1435.8	76.3	$6.608 \pm 0.217$	$6.608 \pm 0.217$
		1009.8	29.8	$6.724 \pm 0.263$	$6.724 \pm 0.263$
		462.8	30.7	$6.651 \pm 0.209$	$6.651 \pm 0.209$
$^{139}\text{Ba}$	83.03 min	165.8	23.7	$6.480 \pm 0.124$	$6.480 \pm 0.124$
$^{140}\text{Ba}$	12.75 d	537.3	24.4	$6.011 \pm 0.258$	$6.011 \pm 0.258$
$^{141}\text{Ce}$	32.5 d	145.4	48.0	$5.268 \pm 0.214$	$5.268 \pm 0.214$
$^{142}\text{La}$	91.1 min	641.3	47.0	$4.489 \pm 0.182$	$4.525 \pm 0.183$
$^{143}\text{Ce}$	33.03 h	293.3	42.8	$4.660 \pm 0.194$	$4.698 \pm 0.195$
$^{144}\text{Ce}$	284.89 d	133.5	11.09	$4.827 \pm 0.204$	$4.827 \pm 0.204$
$^{147}\text{Nd}$	10.98 d	531.0	13.1	$3.620 \pm 0.118$	$3.620 \pm 0.118$
$^{149}\text{Nd}$	1.728 h	211.3	25.9	$2.133 \pm 0.167$	$2.142 \pm 0.168$
		270.2	10.6	$2.004 \pm 0.150$	$2.088 \pm 0.151$
$^{151}\text{Pm}$	53.08 h	340.8	23.0	$0.829 \pm 0.022$	$0.829 \pm 0.022$
$^{153}\text{Sm}$	46.28 h	103.2	30.0	$0.473 \pm 0.027$	$0.473 \pm 0.027$

\* The yields of  $^{115}\text{Cd}^{\text{total}}$  are based on the ratio of  $^{115}\text{Cd}^{\text{g}}/^{115}\text{Cd}^{\text{m}} = 6$  from Ref. [65].  $Y_{\text{R}}$  – cumulative yields,  $Y_{\text{A}}$  – mass yields,  $^{135}\text{I}$  – fission rate monitor.

Table 4

Nuclear spectroscopic data and yields of fission products in the 10.09 MeV neutron-induced fission of  $^{238}\text{U}$ .

Nuclide	Half-life	$\gamma$ -ray		$Y_R$ (%)	$Y_A$ (%)
		Energy (keV)	Abundance (%)		
$^{84}\text{Br}$	31.8 min	1616.2	6.2	$0.825 \pm 0.041$	$0.825 \pm 0.041$
$^{85}\text{Kr}^m$	4.48 h	151.2	75.0	$1.106 \pm 0.079$	$1.103 \pm 0.079$
		304.9	14.0	$1.115 \pm 0.051$	$1.115 \pm 0.051$
$^{87}\text{Kr}$	76.3 min	402.6	49.6	$1.932 \pm 0.096$	$1.934 \pm 0.097$
$^{88}\text{Kr}$	2.84 h	196.3	25.9	$2.445 \pm 0.196$	$2.480 \pm 0.199$
$^{91}\text{Sr}$	9.63 h	749.8	23.6	$4.084 \pm 0.215$	$4.084 \pm 0.215$
		1024.3	33.0	$3.908 \pm 0.206$	$3.908 \pm 0.206$
$^{92}\text{Sr}$	2.71 h	1384.9	90.0	$4.255 \pm 0.188$	$4.260 \pm 0.188$
$^{93}\text{Y}$	10.18 h	266.9	7.3	$3.947 \pm 0.165$	$3.947 \pm 0.165$
$^{95}\text{Zr}$	64.02 d	756.7	54.0	$5.637 \pm 0.154$	$5.637 \pm 0.154$
		724.3	44.2	$5.528 \pm 0.182$	$5.528 \pm 0.182$
$^{97}\text{Zr}$	16.91 h	743.4	93.0	$6.036 \pm 0.295$	$5.557 \pm 0.295$
$^{99}\text{Mo}$	65.94 h	140.5	89.4	$5.205 \pm 0.097$	$5.205 \pm 0.097$
		739.5	12.13	$5.404 \pm 0.102$	$5.404 \pm 0.102$
$^{103}\text{Ru}$	39.26 d	497.1	90.0	$6.125 \pm 0.211$	$6.125 \pm 0.211$
$^{105}\text{Ru}$	4.44 h	724.4	47.0	$3.532 \pm 0.181$	$3.539 \pm 0.181$
$^{105}\text{Rh}$	35.36 h	319.1	19.2	$3.589 \pm 0.148$	$3.589 \pm 0.148$
$^{112}\text{Ag}$	3.13 h	617.5	43.0	$0.512 \pm 0.038$	$0.512 \pm 0.038$
$^{113}\text{Ag}$	5.37 h	298.6	10.0	$0.403 \pm 0.017$	$0.404 \pm 0.017$
$^{115}\text{Cd}^g$	53.46 h	336.2	45.9	$0.290 \pm 0.034$	$0.290 \pm 0.034$
$^{115}\text{Cd}^{\text{total}}$				$0.338 \pm 0.039^*$	$0.338 \pm 0.039^*$
$^{117}\text{Cd}^m$	3.36 h	1066.0	23.1	$0.062 \pm 0.010$	
		1097.3	26.0	$0.057 \pm 0.011$	
$^{117}\text{Cd}^g$	2.49 h	273.4	28.0	$0.220 \pm 0.026$	
$^{117}\text{Cd}^{\text{total}}$				$0.279 \pm 0.028$	$0.279 \pm 0.063$
$^{127}\text{Sb}$	3.85 d	687.0	37.0	$0.774 \pm 0.063$	$0.774 \pm 0.063$
$^{128}\text{Sn}$	59.07 min	482.3	59.0	$0.992 \pm 0.119$	$1.044 \pm 0.125$
$^{129}\text{Sb}$	4.32 h	812.4	43.0	$1.331 \pm 0.074$	$1.335 \pm 0.074$
$^{131}\text{I}$	8.02 d	364.5	81.7	$3.418 \pm 0.211$	$3.418 \pm 0.211$
$^{132}\text{Te}$	3.2 d	228.1	88.0	$5.541 \pm 0.232$	$5.569 \pm 0.233$
$^{133}\text{I}$	20.8 h	529.9	87.0	$6.501 \pm 0.176$	$6.501 \pm 0.176$
$^{134}\text{Te}$	41.8 min	566.0	18.0	$6.838 \pm 0.211$	$7.369 \pm 0.226$
		767.2	29.5	$6.732 \pm 0.296$	$7.254 \pm 0.307$
$^{135}\text{I}$	6.57 h	1131.5	22.7	$5.134 \pm 0.192$	$5.170 \pm 0.193$
		1260.4	28.9	$5.688 \pm 0.056$	$5.728 \pm 0.057$
$^{138}\text{Cs}^g$	33.41 min	1435.8	76.3	$6.371 \pm 0.148$	$6.371 \pm 0.148$
		1009.8	29.8	$6.190 \pm 0.204$	$6.190 \pm 0.204$
		462.8	30.7	$6.161 \pm 0.244$	$6.161 \pm 0.244$
$^{139}\text{Ba}$	83.03 min	165.8	23.7	$5.889 \pm 0.344$	$5.889 \pm 0.344$
$^{140}\text{Ba}$	12.75 d	537.3	24.4	$5.449 \pm 0.232$	$5.449 \pm 0.232$
$^{141}\text{Ce}$	32.5 d	145.4	48.0	$4.863 \pm 0.215$	$4.863 \pm 0.215$
$^{142}\text{La}$	91.1 min	641.3	47.0	$4.486 \pm 0.085$	$4.486 \pm 0.085$
$^{143}\text{Ce}$	33.03 h	293.3	42.8	$4.471 \pm 0.199$	$4.471 \pm 0.199$
$^{144}\text{Ce}$	284.89 d	133.5	11.09	$4.641 \pm 0.206$	$4.641 \pm 0.206$
$^{147}\text{Nd}$	10.98 d	531.0	13.1	$3.811 \pm 0.279$	$3.811 \pm 0.279$
$^{149}\text{Nd}$	1.728 h	211.3	25.9	$2.798 \pm 0.334$	$2.809 \pm 0.336$
		270.2	10.6	$2.821 \pm 0.273$	$2.832 \pm 0.274$
$^{151}\text{Pm}$	53.08 h	340.8	23.0	$0.995 \pm 0.037$	$0.995 \pm 0.037$
$^{153}\text{Sm}$	46.28 h	103.2	30.0	$0.478 \pm 0.034$	$0.478 \pm 0.034$

\* The yields of  $^{115}\text{Cd}^{\text{total}}$  are based on the ratio of  $^{115}\text{Cd}^g/^{115}\text{Cd}^m = 6$  from Ref. [65].  $Y_R$  – cumulative yields,  $Y_A$  – mass yields,  $^{135}\text{I}$  – fission rate monitor.

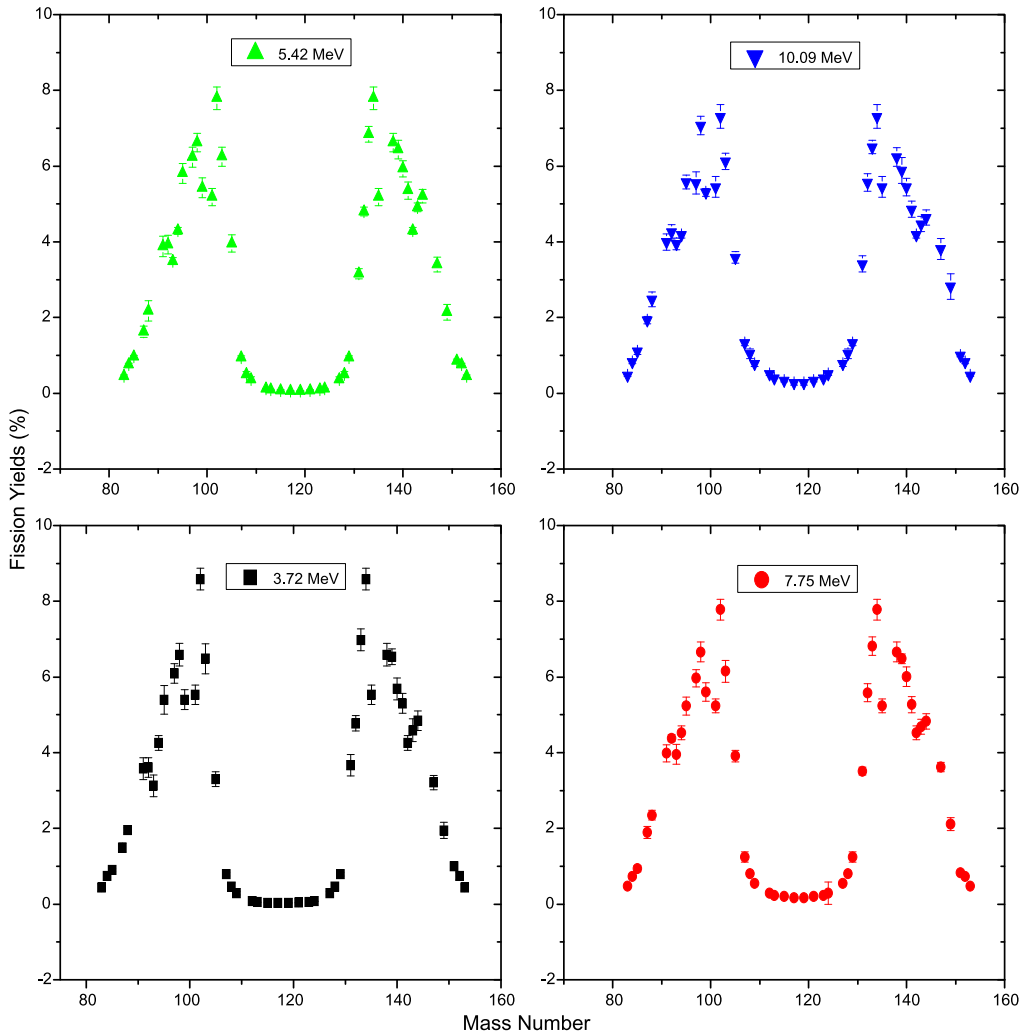


Fig. 1. Plot of mass yields distribution in the 3.72-, 5.42-, 7.75- and 10.09-MeV quasi-mono-energetic neutron-induced fission of  $^{238}\text{U}$ .

#### 4. Discussion

The yields of fission products shown in Table 4 for the neutron-induced fission of  $^{238}\text{U}$  at average neutron energy of 10.09 MeV are determined for the first time. On the other hand, the yields of some of the fission products in the neutron-induced fission of  $^{238}\text{U}$  at 3.72, 5.42 and 7.75 MeV from Tables 1–3 are the re-determined value but are in agreement with the literature data [64–69] at 3.72, 5.5 and 7.7 MeV. The literature data [64–69] are based on purely mono-energetic neutrons, whereas the present data are for average neutron energies based on quasi-mono-energetic neutrons. The mass-chain-yield data in the neutron-induced fission of  $^{238}\text{U}$  from present work at average neutron energies of 3.72, 5.42, 7.75 and 10.09 MeV are plotted in Fig. 1 as a function of their mass number. Similarly, the yields of fission products in the 4.0, 5.9, 8.0 and

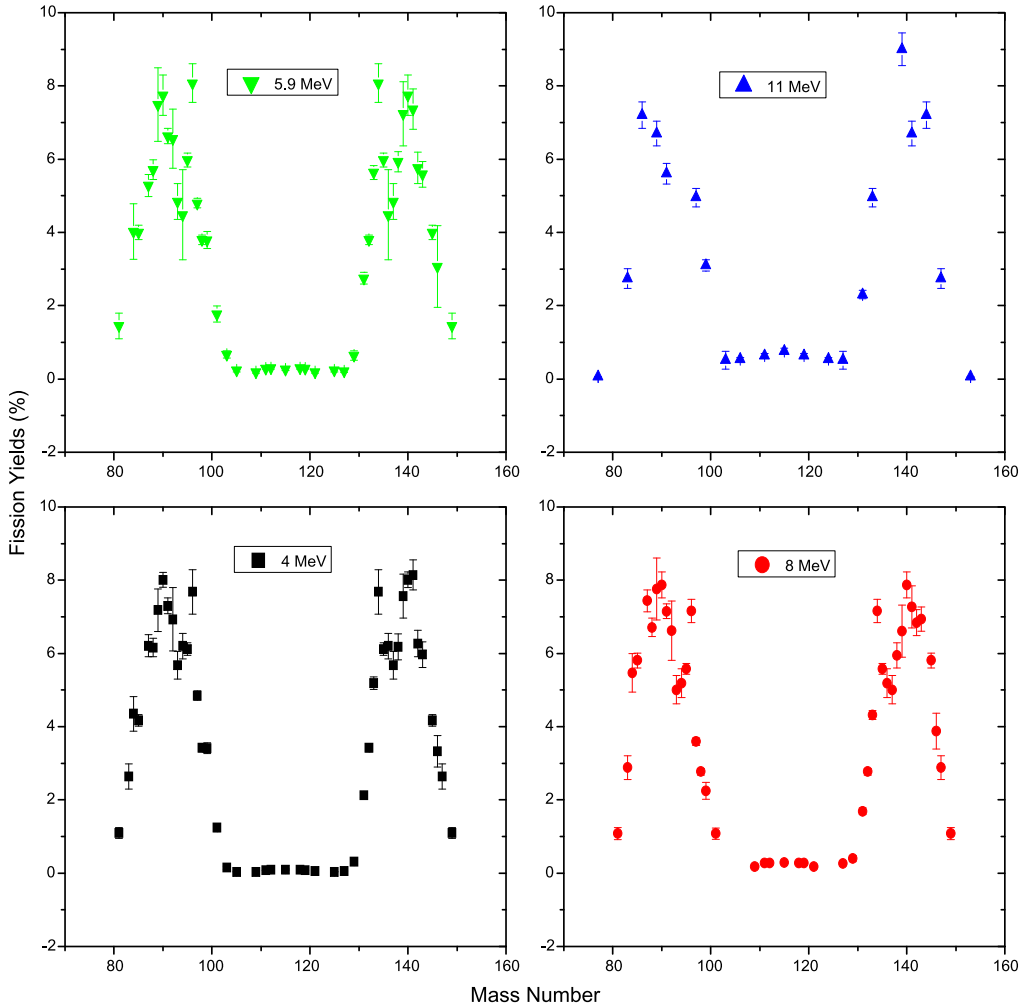


Fig. 2. Plot of mass yields distribution in the 4.0, 5.9, 8.0 and 11.0-MeV neutron-induced fission of  $^{232}\text{Th}$ .

11.0 MeV neutron-induced fission of  $^{232}\text{Th}$  from literature [26,42] of comparable excitation energies are plotted in Fig. 2. This has been done to examine the effect nuclear structure between  $^{238}\text{U}(n, f)$  and  $^{232}\text{Th}(n, f)$  of comparable excitation energy. It was observed from Figs. 1 and 2 that in the neutron-induced fission of  $^{238}\text{U}$  and  $^{232}\text{Th}$ , the yields of fission products for  $A = 133\text{--}134$ ,  $138\text{--}140$  and  $143\text{--}144$  as well as their complementary products are higher than the other fission products. The oscillation in the interval of five mass units is due to the even–odd effect [87]. The higher yields of fission products for  $A = 134\text{--}134$  and  $143\text{--}144$  can also be explained from the point of view of the standard I and standard II asymmetric fission modes as mentioned by Brossa et al. [88], which arise due to shell effects [89]. Based on standard I asymmetry, the fissioning system is characterized by spherical heavy fragment with mass numbers  $133\text{--}134$  due to the spherical  $82$  n shell and a deformed complementary light mass fragment. Based on standard II asymmetry, the fissioning system is characterized by a deformed heavy-mass fragment near the mass numbers of  $143\text{--}144$  due to a deformed  $86\text{--}88$  n shell and slightly deformed light mass

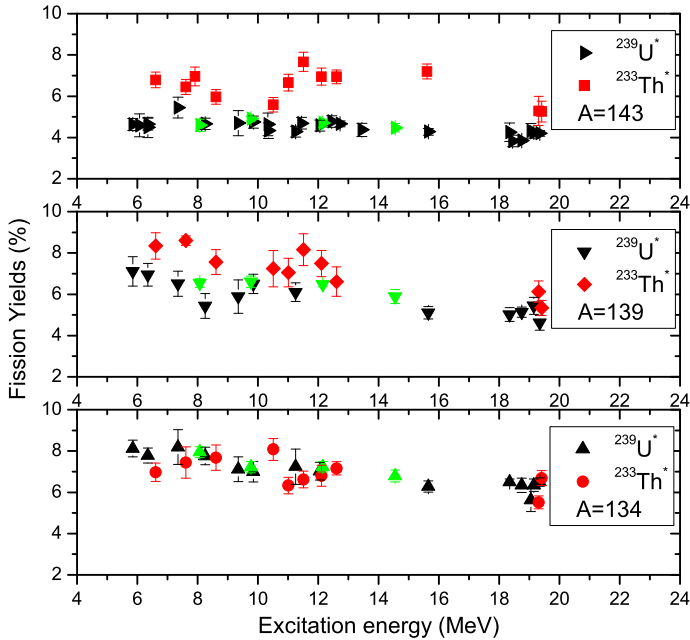


Fig. 3. Plot of yields of fission products (%) as a function of excitation energy for  $A = 143$ ,  $139$  and  $134$  in the  $^{238}\text{U}(n, f)$  and  $^{232}\text{Th}(n, f)$  reactions. The data of present work in  $^{238}\text{U}(n, f)$  are of same symbol with literature data but with green color. (For interpretation of the references to color in this figure legend, the reader is referred to the web version of this article.)

fragment. Thus, the higher yields of fission products for  $A = 133$ – $134$  and  $143$ – $144$  are due to the presence of spherical  $82$  n and deformed  $86$ – $88$  n shells, respectively.

Further, it can be seen from Fig. 1 that in  $^{238}\text{U}(n, f)$ , the yields of fission products for  $A = 133$ – $134$  are higher than for  $A = 138$ – $140$  and  $143$ – $144$ . On the other hand, in  $^{232}\text{Th}(n, f)$ , the yields of fission products for  $A = 138$ – $140$  are higher than for  $A = 133$ – $134$  and  $143$ – $144$  (Fig. 2). In order to examine this aspects, the yields of fission products for  $A = 133$ ,  $139$  and  $143$  from the present work (Tables 1–4) and literature data in the  $^{238}\text{U}(n, f)$  [47–72] and  $^{232}\text{Th}(n, f)$  [25–48] are plotted in Fig. 3 as a function of excitation energy. It can be seen from Fig. 3 that the yields of fission products for  $A = 134$  and their complementary products are comparable or slightly higher at all excitation energy in  $^{238}\text{U}(n, f)$  than in  $^{232}\text{Th}(n, f)$ . On the other hand, the yields of fission products for  $A = 139$  and  $143$  are lower at all excitation energy in  $^{238}\text{U}(n, f)$  than in  $^{232}\text{Th}(n, f)$ . This different behavior between the fissioning systems  $^{239}\text{U}^*$  and  $^{233}\text{Th}^*$  cannot be explained only based on the standard I and standard II asymmetric fission modes unless the shell combination of the complementary fragments are considered. In  $^{238}\text{U}(n, f)$  and  $^{232}\text{Th}(n, f)$ , the fission products for  $A = 134$  and  $139$ – $143$  have the spherical  $82$  n and deformed  $86$ – $88$  n shell if one and two neutron emission are considered. However, the complementary fragment for  $A = 134$  in  $^{238}\text{U}(n, f)$ , has a deformed  $64$  n shell but no shell in  $^{232}\text{Th}(n, f)$ . Thus the slightly higher yield for  $A = 134$  and its complementary product in  $^{238}\text{U}(n, f)$  is due to the presence of spherical  $82$  n and deformed  $64$  n shell combination. Similarly, the complementary fragment for  $A = 139$  formed in the  $^{232}\text{Th}(n, f)$  reaction is characterized by the deformed  $56$  n shell, while no shell is present if produced in the  $^{238}\text{U}(n, f)$  reaction. Thus the higher yield for  $A = 139$  and its complementary product in  $^{232}\text{Th}(n, f)$  is due to the presence of deformed  $86$  n

and 56 n shell combination. For the fragment for  $A = 143$ , in both  $^{232}\text{Th}(n, f)$  and  $^{238}\text{U}(n, f)$  the complementary fragments have no shell. However, in  $^{232}\text{Th}(n, f)$ , for  $A = 143$ , the complementary fragment approaches closer to the spherical 50 n shell and thus the yields are higher. This observation gets support from the highest yield of the fission products pair for  $A = 144$  and 84 in  $^{229}\text{Th}(n, f)$  [90], which is due to the presence of deformed 88 n and spherical 50 n shell combination. These observations indicate that the fission product and its complementary product have highest yield if both complementary fragments pair have shell combination. If one of the fragments of the complementary pair has a shell then the yields are higher. If none of the fragments of the complementary pair has shell then the yields are the lowest.

Besides the above observations, it can be seen from Figs. 1 and 2 that within the average excitation energy of 8–12 MeV of present work, the mass yield distribution in  $^{238}\text{U}(n, f)$  is double humped, whereas it is triple humped in  $^{232}\text{Th}(n, f)$ . This is due to the different type of potential energy surface in  $^{233}\text{Th}^*$  compared to  $^{239}\text{U}^*$  [91]. In order to examine this aspect, the yields of symmetric products, high yield asymmetric products and the peak-to-valley (P/V) ratios from the present work and literature data [48–73] in  $^{238}\text{U}(n, f)$  are shown in Table 5. The yields of high yields fission products and symmetric products in  $^{238}\text{U}(n, f)$  from Table 5 along with the similar literature data [25–48] in  $^{232}\text{Th}(n, f)$  are plotted in Fig. 4 as a function of excitation energy. In  $^{238}\text{U}(n, f)$ , the yield of high-yield asymmetric product is for  $A = 133$  or 134 and for symmetric product, it is for  $A = 115$ . In  $^{232}\text{Th}(n, f)$ , the yields of high-yield asymmetric product is for  $A = 139$  or 140 and for symmetric product, it is for  $A = 113$  or 115 depending on which data available in the literature. In Fig. 5, the P/V ratios from Table 5 in  $^{238}\text{U}(n, f)$  and similar data from literature [25–48] in  $^{232}\text{Th}(n, f)$  are plotted as a function of excitation energy.

It can be seen from Fig. 4 that in both  $^{238}\text{U}(n, f)$  and  $^{232}\text{Th}(n, f)$ , the yields of asymmetric products decrease slightly, whereas the yields of symmetric products increase significantly with excitation energy. This is to conserve the mass yield distribution of 200%. However, it can be seen from Fig. 4 that the yields of symmetric products in  $^{232}\text{Th}(n, f)$  increase sharply up to excitation energy of 10 MeV and then slightly decrease up to 13 MeV and thereafter again increase. Accordingly, in  $^{232}\text{Th}(n, f)$ , the peak-to-valley ratio (Fig. 5) decreases up to 10 MeV and then slightly increases up to 13 MeV and thereafter again decrease. On the other hand, in  $^{238}\text{U}(n, f)$ , the yields of symmetric products (Fig. 4) and decrease of peak-to-valley ratio (Fig. 5) are nearly smooth with excitation energy. The different behavior of  $^{232}\text{Th}(n, f)$  compared to  $^{238}\text{U}(n, f)$  within excitation energy of 10–12.5 MeV is due to the greater effect of giant dipole resonance (GDR) in the former than in the later. Similar effect within excitation energy of 10–13 MeV was also seen in the proton induced fission of  $^{232}\text{Th}$  [92], which supports the present observation. Otherwise, above excitation energy of 7.5 MeV, the yields of symmetric products are higher in  $^{232}\text{Th}(n, f)$  than in  $^{238}\text{U}(n, f)$  and increase with excitation energy (Fig. 4). However, the peak-to-valley ratio is higher in  $^{238}\text{U}(n, f)$  than in  $^{232}\text{Th}(n, f)$  and decreases with excitation energy (Fig. 5). This is due to the different type of potential energy surface in  $^{233}\text{Th}^*$  compared to  $^{239}\text{U}^*$  [90] as mentioned before besides the role of excitation energy.

In order to examine the role of excitation energy, the average values of light mass ( $\langle A_L \rangle$ ) and heavy mass ( $\langle A_H \rangle$ ) in the  $^{238}\text{U}(n, f)$  from the present work at average neutron energies of 3.72, 5.42, 7.75 and 10.09 MeV as well as at other lower energies [48–73] are calculated from the mass-chain yields ( $Y_A$ ) of the fission products within the mass ranges of 80–105 and 125–150, and by using the following relation:

$$\langle A_L \rangle = \sum (Y_A A_L) / \sum Y_A, \quad \langle A_H \rangle = \sum (Y_A A_H) / \sum Y_A \quad (7)$$

Table 5

Yields of asymmetric ( $Y_a$ ) and symmetric ( $Y_s$ ) products and P/V ratio in neutron-induced fission of  $^{238}\text{U}$ .

$E_n$ (MeV)	$E^*$ (MeV)	$Y_a$ (%)	$Y_s$ (%)	P/V ratio	Ref.
1.5	5.85	$8.120 \pm 0.400$	$0.0102 \pm 0.0014$	$796.1 \pm 116.1$	[65]
1.5	5.85	–	$0.0075 \pm 0.0008$	825.0	[51]
1.72	6.07	$7.830 \pm 0.930$	–	–	[69]
2.0	6.35	$7.780 \pm 0.370$	$0.0121 \pm 0.0017$	$643.0 \pm 95.4$	[65]
2.0	6.35	–	$0.0135 \pm 0.0014$	452.0	[51]
2.16	6.55	$7.510 \pm 0.830$	–	–	[69]
3.0	7.35	–	$0.029 \pm 0.003$	238.0	[51]
3.0	7.35	$8.190 \pm 0.840$	$0.034 \pm 0.006$	$240.9 \pm 49.2$	[60]
3.72	8.07	$7.945 \pm 0.267$	$0.038 \pm 0.006$	$209.1 \pm 33.7$	[A]
3.72	8.07	$7.490 \pm 0.790$	–	–	[69]
3.9	8.25	$7.760 \pm 0.420$	$0.034 \pm 0.005$	$228.2 \pm 35.8$	[65]
3.9	8.25	–	$0.047 \pm 0.005$	129.0	[51]
4.78	9.13	$6.770 \pm 0.700$	–	–	[69]
4.8	9.15	–	$0.068 \pm 0.007$	89.0	[51]
5.42	9.77	$7.223 \pm 0.277$	$0.074 \pm 0.018$	$97.6 \pm 24.1$	[A]
5.5	9.85	$7.000 \pm 0.500$	$0.077 \pm 0.011$	$90.9 \pm 14.5$	[65]
5.98	10.33	$6.290 \pm 0.800$	–	–	[69]
6.0	10.35	$6.132 \pm 0.699$	$0.124 \pm 0.010$	$49.5 \pm 6.9$	[68]
6.9	11.25	$7.240 \pm 0.860$	$0.134 \pm 0.018$	$54.0 \pm 9.7$	[65]
7.1	11.45	$6.839 \pm 0.595$	$0.121 \pm 0.009$	$56.5 \pm 6.5$	[68]
7.7	12.05	$7.020 \pm 0.430$	$0.191 \pm 0.032$	$36.8 \pm 6.6$	[65]
7.75	12.1	$7.257 \pm 0.215$	$0.202 \pm 0.037$	$35.9 \pm 6.7$	[A]
8.1	12.45	$6.713 \pm 0.665$	$0.135 \pm 0.011$	$49.7 \pm 6.4$	[68]
8.27	12.72	$7.210 \pm 0.430$	$0.227 \pm 0.009$	$31.2 \pm 1.6$	[67]
9.1	13.45	$6.308 \pm 0.688$	$0.191 \pm 0.016$	$33.0 \pm 4.5$	[68]
10.09	14.55	$6.785 \pm 0.286$	$0.338 \pm 0.039$	$20.1 \pm 2.5$	[A]
11.3	15.65	$6.660 \pm 0.260$	$0.430 \pm 0.050$	$15.5 \pm 1.9$	[70]
13.0	17.35	–	$0.570 \pm 0.070$	8.8	[51]
14.0	18.35	$6.500 \pm 0.150$	$0.860 \pm 0.090$	$7.6 \pm 0.8$	[53]
14.0	18.35	–	$0.970 \pm 0.150$	–	[62]
14.1	18.45	$6.000 \pm 0.210$	$0.950 \pm 0.090$	$6.6 \pm 0.6$	[59]
14.4	18.75	$6.340 \pm 0.340$	$0.843 \pm 0.048$	$7.5 \pm 0.6$	[63]
14.4	18.75	–	$0.975 \pm 0.055$	–	[63]
14.7	19.05	$6.360 \pm 0.450$	$0.860 \pm 0.090$	$7.4 \pm 0.9$	[34]
14.7	19.05	–	$0.930 \pm 0.120$	–	[34]
14.8	19.15	$6.350 \pm 0.300$	$0.870 \pm 0.150$	$7.3 \pm 1.3$	[61]
14.8	19.15	–	$0.950 \pm 0.070$	–	[61]
14.9	19.25	$6.50 \pm 0.300$	$0.985 \pm 0.039$	$6.6 \pm 0.4$	[68]
14.9	19.05	–	$0.834 \pm 0.039$	–	[68]
15.0	19.35	–	$0.780 \pm 0.090$	6.5	[51]
16.4	20.75	–	$0.870 \pm 0.100$	5.8	[51]
17.7	22.05	–	$0.740 \pm 0.090$	6.8	[51]

[A] – Present work.

The  $\langle A_L \rangle$  and  $\langle A_H \rangle$  values obtained from the above relation in the  $^{238}\text{U}(n, f)$  along with their corresponding average excitation energy ( $\langle E^* \rangle$ ) are given in Table 6. From the  $\langle A_L \rangle$ ,  $\langle A_H \rangle$  and compound nucleus mass ( $A_C = 239$ ), the experimental average numbers of neutrons ( $\langle \nu \rangle_{\text{expt}}$ ) were calculated from the following relation:

$$\langle \nu \rangle_{\text{expt}} = A_C - (\langle A_L \rangle + \langle A_H \rangle) \quad (8)$$

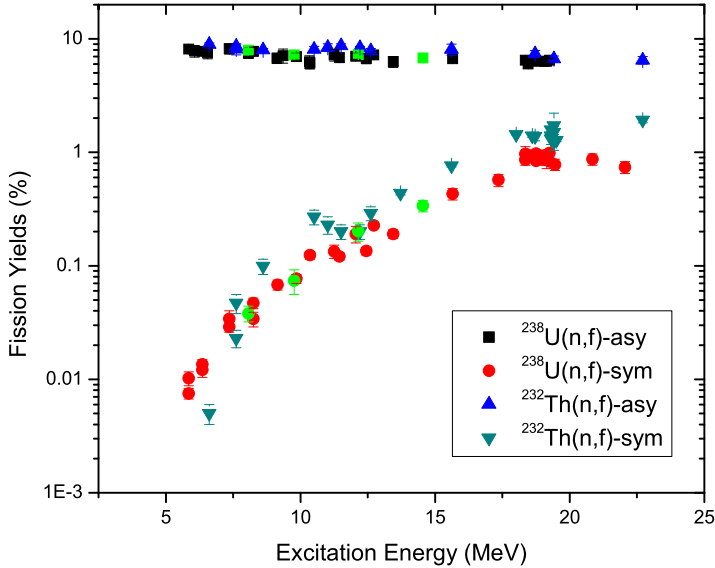


Fig. 4. Plot of yields of symmetric and asymmetric fission products (%) as a function of excitation energy in the neutron-induced fission of  $^{238}\text{U}$  and  $^{232}\text{Th}$ . The data of present work in  $^{238}\text{U}(n, f)$  are of same symbol with literature data but with green color. (For interpretation of the references to color in this figure legend, the reader is referred to the web version of this article.)

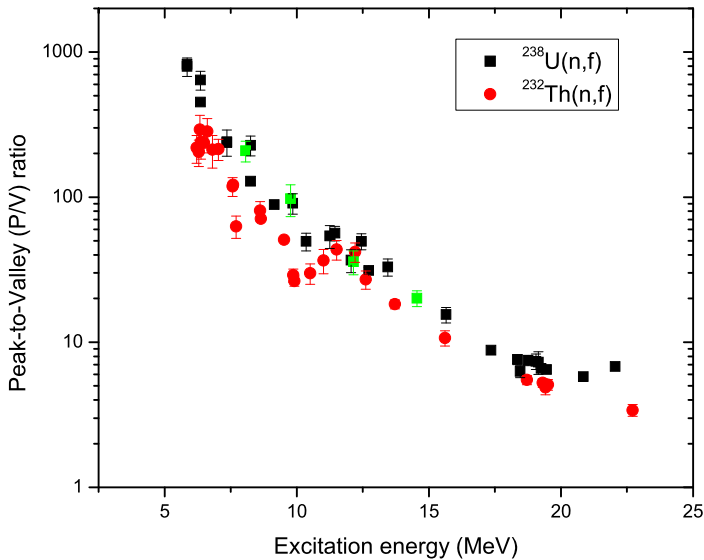


Fig. 5. Plot of peak-to-valley (P/V) ratio as a function of excitation energy in the neutron-induced fission of  $^{238}\text{U}$  and  $^{232}\text{Th}$ . The data of present work in  $^{238}\text{U}(n, f)$  are of same symbol with literature data but with green color. (For interpretation of the references to color in this figure legend, the reader is referred to the web version of this article.)

The  $\langle \nu \rangle_{\text{expt}}$  values obtained from the above relation from the present work and literature data in the  $^{238}\text{U}(n, f)$  [59–69] at different excitation energies are listed in Table 6. The  $\langle \nu \rangle_{\text{expt}}$  values

Table 6

Average light mass ( $\langle A_L \rangle$ ), heavy mass ( $\langle A_H \rangle$ ), and average neutron numbers ( $\langle \nu \rangle_{\text{expt}}$  and  $\langle \nu \rangle_{\text{calc}}$ ) in the neutron-induced fission of  $^{238}\text{U}$ .

$E_n$ (MeV)	$E^*$ (MeV)	$\langle A_L \rangle$	$\langle A_H \rangle$	$\langle \nu \rangle_{\text{expt}}$	Ref.
$^{238}\text{U}(n, f)$					
1.5	5.85	97.5	139	2.5	[65]
2.0	6.35	97.5	139	2.5	[65]
3.0	7.35	97.46	139	2.54	[60]
3.72	8.07	97.44	138.89	2.67	[A]
3.9	8.25	97.4	138.9	2.7	[65]
5.42	9.77	97.27	138.82	2.91	[A]
5.5	9.85	97.4	138.6	3.0	[65]
6.0	10.35	97.44	138.47	3.09	[64]
6.9	11.51	97.5	138.4	3.1	[65]
7.1	11.45	97.4	138.35	3.25	[64]
7.7	11.05	97.4	138.3	3.3	[65]
7.75	12.1	97.37	138.33	3.31	[A]
8.1	12.45	97.48	138.13	3.39	[64]
8.27	12.72	97.4	138.2	3.4	[67]
9.1	13.45	97.4	138.06	3.6	[64]
10.09	14.55	97.37	138.03	3.6	[A]
11.3	15.65	97.51	137.75	3.74	[70]
14.1	18.45	98.09	136.79	4.12	[62]
14.8	19.15	98.0	136.8	4.2	[61]

[A] – Present work.

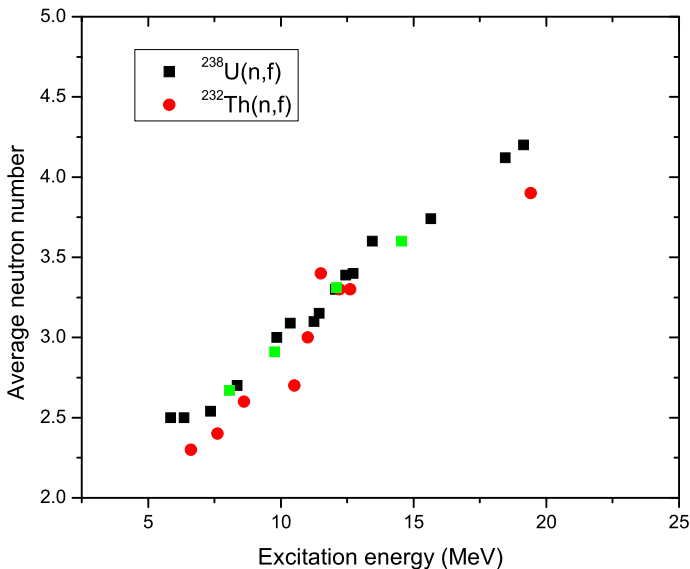


Fig. 6. Plot of average neutron number as a function of excitation energy in the neutron-induced fission of  $^{238}\text{U}$  and  $^{232}\text{Th}$ . The data of present work in  $^{238}\text{U}(n, f)$  are of same symbol with literature data but with green color. (For interpretation of the references to color in this figure legend, the reader is referred to the web version of this article.)

for  $^{238}\text{U}(n, f)$  from Table 6 and literature data [27,42] for  $^{232}\text{Th}(n, f)$  are plotted in Fig. 6 as a function of excitation energy. It can be seen from Fig. 6 that in the neutron-induced fis-

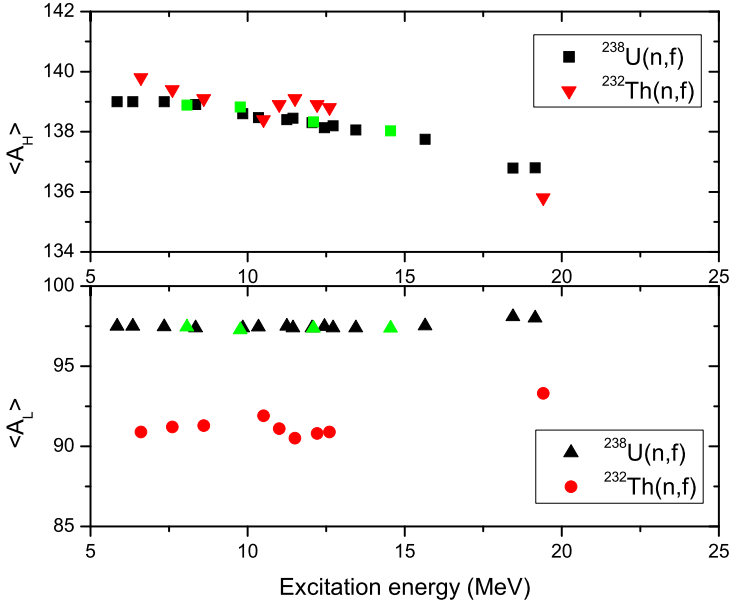


Fig. 7. Plot of average values of heavy mass ( $\langle A_H \rangle$ ) and average values of light mass ( $\langle A_L \rangle$ ) as a function of excitation energy in the neutron-induced fission of  $^{238}\text{U}$  and  $^{232}\text{Th}$ . The data of present work in  $^{238}\text{U}(n, f)$  are of same symbol with literature data but with green color. (For interpretation of the references to color in this figure legend, the reader is referred to the web version of this article.)

sion of  $^{232}\text{Th}$  and  $^{238}\text{U}$ , the value of  $\langle \nu \rangle_{\text{expt}}$  increases with excitation energy. From Fig. 6, it can also be seen that at the same excitation energy, the  $\langle \nu \rangle_{\text{expt}}$  value in  $^{238}\text{U}(n, f)$  is higher than in  $^{232}\text{Th}(n, f)$ , which is due to the effect of fissility parameter besides excitation energy. However, at excitation energy around 11–13 MeV, the value of  $\langle \nu \rangle_{\text{expt}}$  in  $^{232}\text{Th}(n, f)$  is comparable or higher than in  $^{238}\text{U}(n, f)$ , which is due to GDR effect. The  $\langle A_L \rangle$  and  $\langle A_H \rangle$  values in the  $^{238}\text{U}(n, f)$  from Table 6 and literature data [27,42] in the  $^{232}\text{Th}(n, f)$  are plotted in Fig. 7 as a function of excitation energy. It can be seen from Fig. 7 that the  $\langle A_H \rangle$  values for both  $^{238}\text{U}(n, f)$  and  $^{232}\text{Th}(n, f)$  reactions decrease with the excitation energy, whereas, the  $\langle A_L \rangle$  values increase with the excitation energy. However, at all excitation energy, the  $\langle A_H \rangle$  values are lower in  $^{238}\text{U}(n, f)$  than in  $^{232}\text{Th}(n, f)$ , whereas the  $\langle A_L \rangle$  values are significantly higher in  $^{238}\text{U}(n, f)$  than in  $^{232}\text{Th}(n, f)$ . This is due to the mass conservation based on the standards I and II asymmetric mode of fission. Further, it can be seen from Figs. 6 and 7 that the increasing trend of  $\langle \nu \rangle_{\text{expt}}$  and  $\langle A_L \rangle$  and decreasing trend of  $\langle A_H \rangle$  with excitation energy is not smooth in  $^{232}\text{Th}(n, f)$  as in the case of  $^{238}\text{U}(n, f)$ . Within excitation energy of 11–13 MeV, the increasing trend of  $\langle \nu \rangle_{\text{expt}}$  and  $\langle A_L \rangle$  as well as decreasing trend of  $\langle A_H \rangle$  with excitation energy is very sharp. This is due to major GDR effect in  $^{232}\text{Th}(n, f)$  compared to  $^{238}\text{U}(n, f)$ .

## 5. Conclusions

- (i) The yields of fission products in the 3.72-, 5.42-, 7.75- and 10.09-MeV quasi-neutron-induced fission of  $^{238}\text{U}$  were determined by using an off-line  $\gamma$ -ray spectrometric technique. From the yields of various products mass-chain yields were obtained by using charge distribution corrections.

- (ii) The yields of fission products for  $A = 133$ – $134$ ,  $A = 138$ – $140$ , and  $A = 143$ – $144$  and their complementary products in the neutron-induced fission of  $^{238}\text{U}$  and  $^{232}\text{Th}$  are higher than those of other fission products. This is due to shell closure proximity based on standards I and II asymmetric mode of fission besides the role of even–odd effect.
- (iii) Within the excitation energy of present work, the mass yield distributions in the  $^{238}\text{U}(n, f)$  reaction is double humped, whereas that of  $^{232}\text{Th}(n, f)$  reaction is triple humped. This is due to the different type of potential energy surface in  $^{239}\text{U}^*$  than in  $^{233}\text{Th}^*$ .
- (iv) In the neutron-induced fission of  $^{238}\text{U}$  and  $^{232}\text{Th}$ , the yield of high yields asymmetric products decreases marginally, whereas for symmetric products increases sharply with excitation energies. Accordingly, the P/V ratio in both the cases decreases with excitation energy. This shows the role of excitation energy.
- (v) In  $^{238}\text{U}(n, f)$ , the yields of symmetric fission products increases smoothly with excitation energy. On the other hand, in  $^{232}\text{Th}(n, f)$ , the yields of symmetric products increases sharply within excitation energy of 10 MeV and then decreases up to 12.5 MeV and thereafter again increases with excitation energy.
- (vi) At all excitation energies, the P/V ratio in the neutron-induced fission of  $^{238}\text{U}$  are higher than the same for  $^{232}\text{Th}$ , which is due to the different type of potential surface between two fissioning systems. In both  $^{238}\text{U}(n, f)$  and  $^{232}\text{Th}(n, f)$ , the  $\langle \nu \rangle$  and  $\langle A_L \rangle$  values increase and  $\langle A_H \rangle$  values decrease with excitation energies. However, within excitation energy of 10–13 MeV, the increasing trends of  $\langle \nu \rangle$  and  $\langle A_L \rangle$  and decreasing trend of  $\langle A_H \rangle$  with excitation energy is very sharp. This is due to major GDR effect in the  $^{232}\text{Th}(n, f)$  reaction than in the  $^{238}\text{U}(n, f)$  reaction.

## References

- [1] R. Vandenbosch, J.R. Huizenga, *Nuclear Fission*, Academic, New York, 1973.
- [2] C. Wagemans, *The Nuclear Fission Process*, CRC, London, 1990.
- [3] F. Carminati, R. Klapisch, J.P. Revol, J.A. Rubia, C. Rubia, CERN/AT/93-49 (ET) 1993.
- [4] C. Rubia, J.A. Rubio, S. Buono, F. Carminati, N. Fietier, J. Galvez, C. Geles, Y. Kadi, R. Klapisch, P. Mandrillon, J.P. Revol, Ch. Roche, CERN/AT/95-44 (ET) 1995, CERN/AT/95-53(ET) 1995, CERN/LHC/96-01 (LET) 1996, CERN/LHC/97-01 (EET) 1997.
- [5] C.D. Bowman, in: *Proc. of Int. Conf. on Accelerator-Driven Transmutation Technologies and Applications*, Las Vegas, NV, USA, in: AIP Conf. Proc., vol. 346, AIP Publishing, 1994.
- [6] *Accelerator driven systems: Energy generation and transmutation of nuclear waste*, Status report, IAEA-TECDO-985, IAEA, Vienna, November 1997.
- [7] C.D. Bowman, *Annu. Rev. Nucl. Part. Sci.* 48 (1998) 505.
- [8] S. Ganesan, *Pramana J. Phys.* 68 (2007) 257.
- [9] R.K. Sinha, A. Kakodkar, *Nucl. Eng. Des.* 236 (7–8) (2006) 683.
- [10] S. Ganesan, Creation of Indian experimental benchmarks for thorium fuel cycle, IAEA Coordinated research project on “Evaluated data for thorium–uranium fuel cycle”, in: Third Research Co-ordination Meeting, 30 January to 2 February 2006, Vienna, Austria, INDC (NDS)-0494, 2006.
- [11] IAEA-TECDOC-1319: Thorium fuel utilization, options and trends, Fast Reactors and Accelerator Driven Systems Knowledge Base.
- [12] L. Mathieu et al., Proportion for a very simple thorium molten salt reactor, in: *Proc. Global International Conference*, Tsukuba, Japan, 2005, paper No. 428.
- [13] A. Nuttin, D. Heuer, A. Biliebaud, R. Brissot, C. Le Brun, E. Liatard, J.M. Loiseaux, L. Mathieu, O. Meplan, E. Merle-Lucotte, H. Nifenecker, F. Perdu, S. David, Potential of thorium molten salt reactors: Detailed calculations and concept evolution with a view to large scale energy production, *Proc. Nucl. Energy* 46 (2005) 77.
- [14] T.R. Allen, D.C. Crawford, Lead-cooled fast reactor systems and the fuels and materials challenges, *Sci. Technol. Nuclear Installations* (2007), Article ID 97486.
- [15] Annual Project Status Report 2000, MIT-ANP-PR-071, INEFL/EXT-2009-00994.

- [16] E.A.C. Crouch, *At. Data Nucl. Data Tables* 19 (1977) 417.
- [17] B.F. Rider, *Compilation of fission products yields*, NEDO, 12154 3c ENDF-327, Valecicecitos Nuclear Centre, 1981.
- [18] J.R. England, B.F. Rider, *Evaluation and compilation of fission products yields*, ENDF/BVI, 1989, 1992.
- [19] M. James, R. Mills, *Neutron fission products yields*, UKFY2 1991, JEF-2.2 1993.
- [20] A.C. Wahl, *At. Data Nucl. Data Tables* 39 (1988) 1.
- [21] R.H. Iyer, C.K. Mathews, N. Ravindran, K. Rengan, D.V. Singh, M.V. Ramaniah, H.D. Sharma, *J. Inorg. Nucl. Chem.* 25 (1963) 465.
- [22] H.N. Erten, A. Grutter, E. Rossler, H.R. von Gunten, *Nucl. Sci. Eng.* 79 (1981) 167.
- [23] H. Naik, A.G.C. Nair, P.C. Kalsi, A.K. Pandey, R.J. Singh, A. Ramaswami, R.H. Iyer, *Radiochim. Acta* 75 (1996) 69.
- [24] R.H. Iyer, H. Naik, A.K. Pandey, P.C. Kalsi, R.J. Singh, A. Ramaswami, A.G.C. Nair, *Nucl. Sci. Eng.* 135 (2000) 227.
- [25] A. Turkevich, J.B. Niday, *Phys. Rev.* 84 (1951) 52.
- [26] A. Turkevich, J.B. Niday, A. Tompkins, *Phys. Rev.* 89 (1953) 552.
- [27] K.M. Broom, *Phys. Rev.* 133 (1964) B874.
- [28] G.P. Ford, R.B. Leachman, *Phys. Rev. B* 137 (1965) 826.
- [29] R. Ganapathy, P.K. Kuroda, *J. Inorg. Nucl. Chem.* 28 (1966) 2071.
- [30] Tin Mo, M.N. Rao, *J. Inorg. Nucl. Chem.* 30 (1968) 345.
- [31] M. Thin, M.N. Rao, P.K. Kurdo, *J. Inorg. Nucl. Chem.* 30 (1968) 1145.
- [32] A.I. Sagachev, V.G. Vorobeieva, B.D. Kuzminov, V.B. Mikhaylov, Z. Tarsko, *Sov. J. Nucl. Phys.* 7 (1968) 475.
- [33] S.J. Lyle, J. Sellaars, *Radiochim. Acta* 12 (1969) 43.
- [34] L.H. Gevaert, R.E. Jervis, H.D. Sharma, *Can. J. Chem.* 48 (1970) 641.
- [35] J. Blachot, L.C. Carraz, P. Cavallini, E. Monmand, F. Schusslor, *J. Radioanal. Nucl. Chem.* 7 (1971) 309.
- [36] D.L. Swindle, D.T. Moore, J.N. Beck, P.K. Kuroda, *J. Inorg. Nucl. Chem.* 33 (1971) 3643.
- [37] W. Holubarsch, L. Pfeiffer, F. Gonnenwein, *Nucl. Phys. A* 171 (1971) 631.
- [38] S.A. Rao, *Phys. Rev.* 5 (1972) 171.
- [39] J.p. Bocquet, R. Brissot, J. Crancon, A. Moussa, *Nucl. Phys. A* 189 (1972) 556.
- [40] S.M. Dubrovina, V.I. Novgorodtseva, L.N. Morozov, V.A. Pchelin, L.V. Chistyakov, V.A. Schigin, V.M. Shubko, *Yad. Fiz.* 17 (1973) 1470.
- [41] J. Trochon, H.A. Yehia, F. Brisard, Y. Pranal, *Nucl. Phys. A* 318 (1979) 63.
- [42] L.E. Glendenin, J.E. Gindler, I. Ahmad, D.J. Henderson, J.W. Meadows, *Phys. Rev. C* 22 (1980) 152.
- [43] S.T. Lam, L.L. Yu, H.W. Fielding, W.K. Dawson, G.C. Neilson, *Phys. Rev. C* 28 (1983) 1212.
- [44] A.E. Richoortson, H.L. Wright, J.L. Meason, J.R. Smith, *Nucl. Sci. Eng.* 94 (1986) 413.
- [45] Li Wenxin, Sun Tongyu, Sun Xiuhua, Fu Ming, Dong Tianrong, *High Energy Phys. Nucl. Phys.* 11 (1987) 376.
- [46] Su Tongyu, Li Wenxin, Dong Tianrong, Fu Ming, *High Energy Phys. Nucl. Phys.* 12 (1988) 221.
- [47] V.D. Simutkin, I.V. Ryzhov, G.A. Tutin, L.A. Vaishnene, J. Blongren, S. Pomp, M. Österlund, P. Andersson, R. Bevilacqua, J.P. Meulders, R. Prieels, *Conf. Proc. Amer. Inst. Phys. USA* 1175 (2010) 393.
- [48] I.V. Ryzhov, S.G. Yavshits, G.A. Tutin, N.V. Kovalev, A.V. Saulski, N.A. Kudryashev, A.V. Saulski, N.A. Kudryashev, M.S. Onegin, L.A. Vaishnene, Yu.A. Gavrikov, O.T. Grudzevich, V.D. Simutkin, S. Pomp, J. Blongren, M. Österlund, P. Andersson, R. Bevilacqua, J. Meulders, R. Prieels, *Phys. Rev. C* 85 (2011) 054603.
- [49] K.M. Brown, *Phys. Rev.* 126 (1962) 627.
- [50] M.P. Menon, P.K. Kurdo, *J. Inorg. Nucl. Chem.* 26 (1964) 40.
- [51] N.L. Borisova, S.M. Dubrovina, V.I. Novgorodtseva, V.A. Pchelin, V.A. Shigin, V.M. Shubko, *Sov. J. Nucl. Phys.* 6 (1968) 331.
- [52] S.J. Lyle, J. Tillars, *Radiochim. Acta* 12 (1969) 43.
- [53] D.J. Gorman, R.H. Tomilson, *Can. J. Chem.* 46 (1968) 1663.
- [54] S.J. Lyle, J. Sellaars, *Radiochim. Acta* 12 (1968) 43.
- [55] S.J. Lyle, R. Wellum, *Radiochim. Acta* 13 (1969) 167.
- [56] S.G. Birgul, S.J. Lyle, R. Wellum, *Radiochim. Acta* 16 (1971) 104.
- [57] J.P. Bocquet, *Nucl. Phys.* 189 (1972) 556.
- [58] D.R. Nethaway, B. Mendoza, *Phys. Rev. C* 6 (1972) 1821, 1827.
- [59] J. Blachot, L.C. Carraz, P. Cavalini, C. Chauvin, A. Ferrieu, A. Moussa, *J. Inorg. Nucl. Chem.* 36 (1974) 495.
- [60] J.T. Harvey, D.E. Adams, W.D. James, J.N. Beck, J.L. Meason, P.K. Kuroda, *J. Inorg. Nucl. Chem.* 37 (1975) 2243.
- [61] D.E. Adams, W.D. James, J.N. Beck, P.K. Kuroda, *J. Inorg. Nucl. Chem.* 37 (1975) 419.
- [62] M. Rajagopalan, H.S. Pruys, A. Grutter, E.A. Hermes, H.R. von Gunten, *J. Inorg. Nucl. Chem.* 38 (1976) 351.

- [63] S. Daroczy, P. Raics, S. Nagy, L. Koeber, I. Hamvas, E. Gorman, *Atomki Cozcmenyek* 18 (1976) 317.
- [64] T.C. Chapman, G.A. Anzelon, G.C. Spitalo, D.R. Nethaway, *Phys. Rev. C* 17 (1978) 1089.
- [65] S. Nagy, K.F. Flynn, J.E. Gindler, J.W. Meadows, L.E. Glendenin, *Phys. Rev. C* 17 (1978) 163.
- [66] L. Wexin, S. Tongyu, Z. Manjiao, D. Tianrong, S. Xiuhua, He Huaxue, Yu F. Huakue, *High Energy Phys. Nucl. Phys.* 2 (1980) 9;  
L. Wexin, S. Tongyu, Z. Manjiao, D. Tianrong, S. Xiuhua, He Huaxue, Yu F. Huakue, *High Energy Phys. Nucl. Phys.* 5 (1983) 176.
- [67] L. Ze, Z. Chunhua, L. Conggui, W. Xiuzhi, Q. Limkun, C. Anzhi, L. Huijung, Z. Sujing, L. Yonghui, J. Changxin, L. Daming, T. Peija, M. Jiangchen, J. Kixing, *High Energy Phys. Nucl. Phys.* 7 (1985) 97.
- [68] L. Conggui, L. Huijun, L. Yonghui, *High Energy Phys. Nucl. Phys.* 7 (1985) 235.
- [69] A. Afarideh, K.R. Annole, *Ann. Nucl. Energy* 16 (1989) 313.
- [70] Z. Li, X. Wang, K. Jing, A. Cui, D. Liu, S. Su, P. Tang, T. Chih, S. Zhang, J. Gao, *Radiochim. Acta* 64 (1994) 95.
- [71] G. Lhersonnau, P. Denloov, G. Canchel, J. Huikari, J. Jardin, A. Tokinen, V. Kolhinen, C. Lau, L. Lebroton, A.C. Mueller, A. Nieminen, S. Nummela, H. Penttila, K. Perajavi, Z. Radivojevic, V. Rubchenya, M.G. Saint-Laurent, W.H. Trzaska, D. Vakhtin, J. Vervier, A.C. Villari, J.C. Viang, J. Aystoe, *Eur. Phys. J. A (Hadron and Nuclei)* 9 (2000) 385.
- [72] I. Clenk, *Radiochim. Acta* 85 (1999) 85 (2001) 481;  
I. Clenk, *Radiochim. Acta* 85 (1999) 89 (2001) 481.
- [73] J. Laurec, A. Adam, T. DeBruyne, E. Brauge, T. Granier, J. Aupiais, O. Barsillon, G. Lepetit, N. Authier, P. Casoli, *Nuclear Data Sheet (USA)* 111 (2010) 2965.
- [74] K.-H. Schmidt, S. Steinhäuser, C. Bockstiegel, A. Rewe, A. Heinz, A.R. Junghans, J. Benlliure, H.-G. Clerc, M. de Jong, J. Müller, M. Pfützner, B. Voss, *Nucl. Phys. A* 665 (2000) 221.
- [75] S. Steinhäuser, J. Benlliure, C. Bockstiegel, H.-G. Clerc, A. Heinz, A. Rewe, M. de Jong, A.R. Junghans, J. Müller, M. Pfützner, K.-H. Schmidt, *Nucl. Phys. A* 634 (1998) 89.
- [76] J. Benlliure, A.R. Junghans, K.-H. Schmidt, *Eur. Phys. J. A* 13 (2002) 93.
- [77] H. Umezawa, S. Baba, H. Baba, *Nucl. Phys. A* 160 (1971) 65.
- [78] H. Naik, S.V. Suryanarayana, V.K. Mulik, P.M. Prajapati, B.S. Shivashankar, K.C. Jagadeesan, S.V. Thakare, D. Raj, S.C. Sharma, P.V. Bhagwat, S.D. Dhole, V.N. Bhoraskar, A. Goswami, *J. Radioanal. Nucl. Chem.* 293 (2012) 469.
- [79] V.K. Mulik, S.V. Suryanarayana, H. Naik, S. Mukerji, B.S. Shivashankar, P.M. Prajapati, S.D. Dhole, V.N. Bhoraskar, S. Ganesan, A. Goswami, *Annal. Nucl. Energy*, in press.
- [80] J.F. Ziegler, J.P. Biersack, U. Littmark, *SRIM 2003 Code. The stopping and Range of Ions in Solids*, Pergamon, New York, 2003.
- [81] H. Liskien, A. Paulsen, *At. Data Nucl. Data Tables* 15 (1975) 57.
- [82] J.W. Meadows, D.L. Smith, Neutrons from proton bombardment of natural lithium, Argonne National Laboratory report ANL-7983, 1972.
- [83] C.H. Poppe, J.D. Anderson, J.C. Davis, S.M. Grimes, C. Wong, *Phys. Rev. C* 14 (1976) 438.
- [84] E. Browne, R.B. Firestone, in: V.S. Shirley (Ed.), *Table of Radioactive Isotopes*, Wiley, New York, 1986;  
R.B. Firestone, L.P. Ekstrom, in: *Table of Radioactive Isotopes*, Version 2.1, 2004.
- [85] J. Blachot, C. Fiche, *Ann. Phys. Suppl.* 6 (1981) 3.
- [86] N. Sugarman, A. Turkevich, in: C.D. Coryell, N. Sugarman (Eds.), *Radiochemical Studies: The Fission Product*, vol. 3, McGraw-Hill, New York, 1951, p. 1396.
- [87] H. Naik, R.J. Singh, R.H. Iyer, *Eur. Phys. J. A* 16 (2003) 495.
- [88] U. Brossa, S. Grossmann, A. Müller, *Phys. Rep.* 197 (1990) 167.
- [89] B.D. Wilkins, E.P. Steinberg, R.R. Chasman, *Phys. Rev. C* 14 (1976) 1832.
- [90] C. Agarwal, A. Goswami, P.C. Kalsi, S. Singh, A. Mhatre, A. Ramaswami, *J. Radioanal. Nucl. Chem.* 275 (2008) 445.
- [91] P. Møller, *Nucl. Phys. A* 192 (1972) 529.
- [92] H. Kudo, H. Muramatsu, H. Nakahara, K. Miyano, I. Kohno, *Phys. Rev. C* 25 (1982) 3011.